

Figure 5. FC power control characteristics of the prototype system at p_{FCREF} = 500 W, ν_{Bus} = 120 V, ν_{CI} = 60 V, ν_{FC} = 34.0 V, and i_{FC} = 14.7 A.

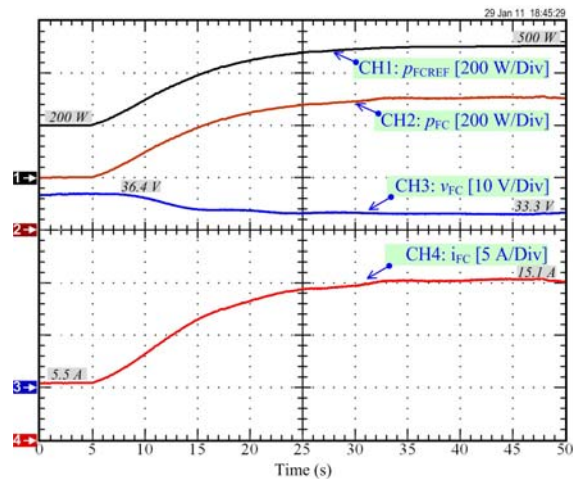


Figure 6. Converter response during the FC power reference trajectory increase from $200~\mathrm{W}$ to $500~\mathrm{W}$.

The data show the dc bus voltage $v_{\rm Bus}$, the output capacitor voltage $v_{\rm C1}$, the output capacitor voltage $v_{\rm C2}$, the FC power reference trajectory $p_{\rm FCREF}$, the measured FC power $p_{\rm FC}$, the FC voltage $v_{\rm FC}$, and the FC current $i_{\rm FC}$. In the initial state, the FC power reference is equal to 500 W, the measured FC power is equal to 500 W, the FC voltage is equal to 33.3 V, the FC current is equal to 15.0 A, the dc bus voltage, and the output capacitor voltages are equal to 118 V and 59.0 V, respectively. At t=10 s, the FC power reference trajectory slowly decreases to the final constant power of 200 W. Again, the measured FC power follows its reference perfectly. It shows the behavior of the balancing system during transient state due to the power reference variation. This result shows that the voltage balancing control is still efficient during transient state.

V. CONCLUSION

A step-up three-level converter topology (high gain transformer-less) with a new control approach based on the differential flatness theory has been proposed for FC applications. Using the nonlinear-control approach based on

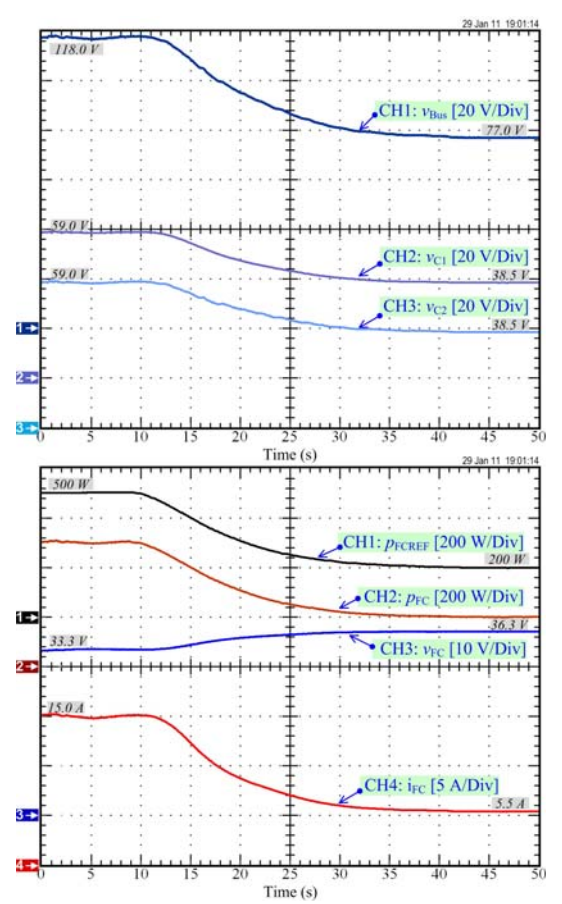


Figure 7. Converter response during the FC power reference trajectory decrease from 500 W to 200 W.

the flatness property, we have proposed a simple solution to the optimization and stabilization problems in the nonlinear power-electronic system. This is the original concept for this kind of application.

A prototype FC converter of 1.2 kW has been designed, and the presented solution has been experimentally verified in the laboratory. The prototype has been tested, and the experimental results have been presented and discussed. The results demonstrate good agreement with the theoretical analysis given in the paper.

REFERENCES

- [1] J. S. Lai and D. J. Nelson, "Energy management power converters in hybrid electric and fuel cell vehicles," *Proc. IEEE*, vol. 95, no. 4, pp. 766–777, April 2007.
- [2] P. Thounthong, B. Davat, S. Raël, and P. Sethakul, "Fuel cell high-power applications," *IEEE Ind. Electron. Mag.*, vol. 3, no. 1, pp. 32–46, March 2009.
- [3] P. J. Grbović, P. Delarue, P. Le Moigne, and P. Bartholomeus, "A bidirectional three-level DC–DC converter for the ultracapacitor applications," *IEEE Trans. Ind. Electron.*, vol. 57, no. 10, pp. 3415– 3430, Oct. 2010.
- [4] E. Song, A. F. Lynch, and V. Dinavahi. "Experimental validation of nonlinear control for a voltage source converter," *IEEE Trans. Control Syst. Technol.*, vol. 17, no. 5, pp. 1135–1144, Sept. 2009.
- [5] A. Gensior, H. Sira-Ramirez, J. Rudolph, and H. Guldner, "On some nonlinear current controllers for three-phase boost rectifiers," *IEEE Trans. Ind. Electron.*, vol. 56, no. 2, pp. 360–370, Feb. 2009.

Fuzzy Control Law Based-on Flatness Property for a DC Link Stabilization for a Fuel Cell/ Supercapacitor Hybrid Power Plant

A. Luksanasakul*, P. Koseeyaporn*, P. Sethakul*, B. Davat**, and P. Thounthong*

*Renewable Energy Research Centre, Department of Teacher Training in Electrical Engineering, King Mongkut's University of Technology North Bangkok, 1518, Pibulsongkram Road, Bangsue, Bangkok, 10800, Thailand. e-mail: thounthong@ieee.org, phtt@kmutnb.ac.th

**Groupe de Recherche en Electrotechnique et Electronique de Nancy, INPL-Nancy University, 2 avenue de la Forêt de Haye, 54516 Vandoeuvre lès Nancy, France,

Abstract--This paper presents a fuzzy control law based on differential flatness approach for distributed dc generation (nonlinear system) supplied by a fuel cell (FC) (main source) and supercapacitor (auxiliary source). The main technical feeble point of FCs is slow dynamics because the power slope is limited to prevent fuel starvation problems, improve performance and increase lifetime. The very fast power response and high specific power of a supercapacitor complements the slower power output of the main source to produce the compatibility and performance characteristics needed in a load. The energy in the system is balanced by dc bus energy regulation (or indirect voltage regulation). A supercapacitor module functions by supplying energy to regulate the dc bus energy. The FC, as a slow dynamic source in this system, supplies energy to the supercapacitor module in order to keep it charged. Using the intelligent fuzzy control law based on the flatness property, we propose straightforward solutions to hybrid energy management, dynamic and stabilization problems. To validate the proposed method, a hardware system is realized with analog circuits, and digital estimation is accomplished with a dSPACE controller. Experimental results with small-scale power plant (a polymer electrolyte membrane FC of 1200 W, 46 A and a supercapacitor module of 100 F, 500 A, and 32 V) in a laboratory corroborate the excellent control scheme during a load

Index Terms--Converters, fuel cells, fuzzy logic, supercapacitor, voltage control

I. INTRODUCTION

Currently, interest in FCs has increased sharply, and progress towards commercialization has accelerated. Practical FC systems are becoming obtainable and are expected to capture a growing share of the markets for automotive power [1] and generation equipment [2] once costs fall to competitive levels.

It is indispensable to point out that FCs do not store

This work was supported in part by a research program in cooperation with the Thai–French Innovation Institute, King Mongkut's University of Technology North Bangkok (KMUTNB), and the Institut National Polytechnique de Lorraine, Nancy University, under the Franco-Thai Higher Education and Research Joint Project (2009–2010), and by the Thailand Research Fund (TRF) under Grant MRG5380261.

energy. Energy is stored in the hydrogen gas. The principle of the FC is to convert the energy stored within the hydrogen into electricity. In this way, energy stored within the hydrogen gas is directly converted into electricity [2]. As a result, a given FC design can only supply a limited amount of power in excess of its rating. This means that a FC may not be able to start a high-inrush load such as a motor.

What is needed is to combine the fuel cell with an intermediate energy-storage element that possesses sufficient energy and has the capability to deliver large amounts of power. Two different types of components have been identified that would function to provide the necessary power buffer between the fuel cell and the and supercapacitor lead-acid batteries (ultracapacitors). A lead-acid battery (the sensitivity to temperature, maintenance issues, and limited cycle life) is not the best choice for integration within an FC in a quality system. For this application, supercapacitors are chosen as the energy storage device

This kind of system is a multiconverter structure and exhibits nonlinear behavior. In most control techniques, a mathematical model of systems is exploited to obtain a solution to the feedback regulation problems. The most common structure is a linear structure in which the properties of a linear control system can be used. If the considered system is nonlinear, obtaining favorite results is possible by different linearization around different operating points [3]. Nonetheless, there are situations where this technique offers limited performance. Such situations may include the requirement for tight tracking of the reference signal in spite of large and sudden load variations or fast and smooth equilibrium-to-equilibrium transfers of the converters [4].

In this paper, an intelligent fuzzy logic control algorithm based on the flatness estimation method of the system is proposed. Flatness provides a convenient framework for meeting a number of performance specifications for the hybrid power source [5]. It will provide a significant contribution to the field of the

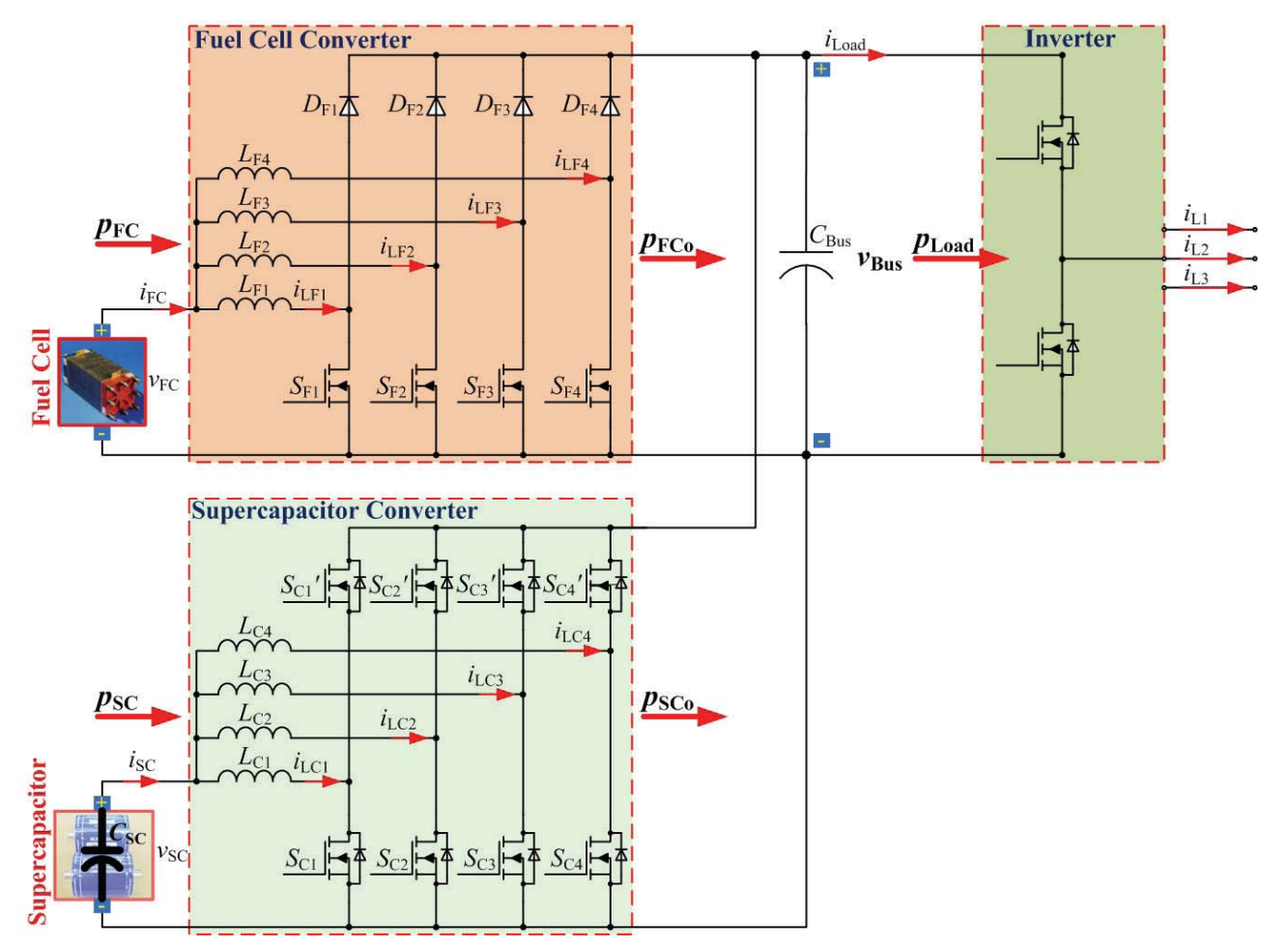


Fig. 1. Proposed circuit diagram of a distributed cogeneration system supplied by a fuel cell and supercapacitor, where p_{Load} (= $v_{\text{Bus}} \times i_{\text{Load}}$), v_{Bus} , and i_{Load} are the load power, the dc bus voltage, and the dc bus load current, respectively. p_{FC} (= $v_{\text{FC}} \times i_{\text{FC}}$), v_{FC} , and i_{FC} are the fuel cell power, voltage, and current, respectively. p_{SC} (= $v_{\text{SC}} \times i_{\text{SC}}$), v_{SC} , and i_{SC} are the supercapacitor power, voltage, and current, respectively. p_{FCo} , and p_{SCo} are the output powers to the DC link from the converters of fuel cell and supercapacitor, respectively.

hybrid power plant, particularly in nonlinear power electronics applications.

II. HYDROGEN ENERGY POWER PLANT

A. Proposed Converter Structure

Fig. 1 depicts the proposed renewable energy power plant. The FC converter is 4-phase boost converters in parallel and the supercapacitor converter is 4-phase bidirectional converters (2-quadrant) in parallel. These parallel connected converters, with interleaved switching technique, increase the power processing capability and availability of the power electronic system [6].

For safety and high dynamics, the FC and supercapacitor converters are primarily controlled by inner current regulation loops, classically. These current control loops are supplied by three reference signals: the supercapacitor current reference $i_{\rm SCREF}$ and the FC current reference $i_{\rm FCREF}$, generated by the energy management algorithm presented hereafter.

B. Converter Modeling

We suppose that the FC and supercapacitor currents

follow their reference values completely. Thus,

$$i_{\text{FC}} = i_{\text{FCREF}} = \frac{p_{\text{FC}}}{v_{\text{FC}}} = \frac{p_{\text{FCREF}}}{v_{\text{FC}}} \tag{1}$$

$$i_{\text{SC}} = i_{\text{SCREF}} = \frac{p_{\text{SC}}}{v_{\text{SC}}} = \frac{p_{\text{SCREF}}}{v_{\text{SC}}}$$
 (2)

Now, the FC generator and the supercapacitor storage device function as controlled current sources. We consider here that there are only static losses in these converters, and $r_{\rm FC}$ and $r_{\rm SC}$ represent static losses in the FC and supercapacitor converters, respectively.

The dc bus capacitive energy y_{Bus} , and the supercapacitive energy y_{SC} can be written as:

$$y_{\text{Bus}} = \frac{1}{2} C_{\text{Bus}} v_{\text{Bus}}^2, \quad y_{\text{SC}} = \frac{1}{2} C_{\text{SC}} v_{\text{SC}}^2$$
 (3)

The total electrostatic energy y_T stored in the dc bus capacitor C_{Bus} and the supercapacitor C_{SC} can also be written as:

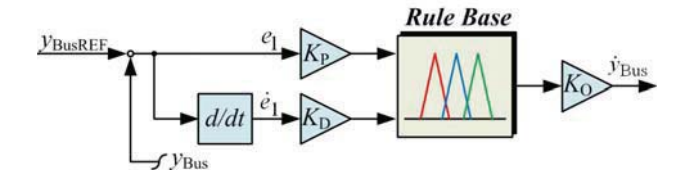
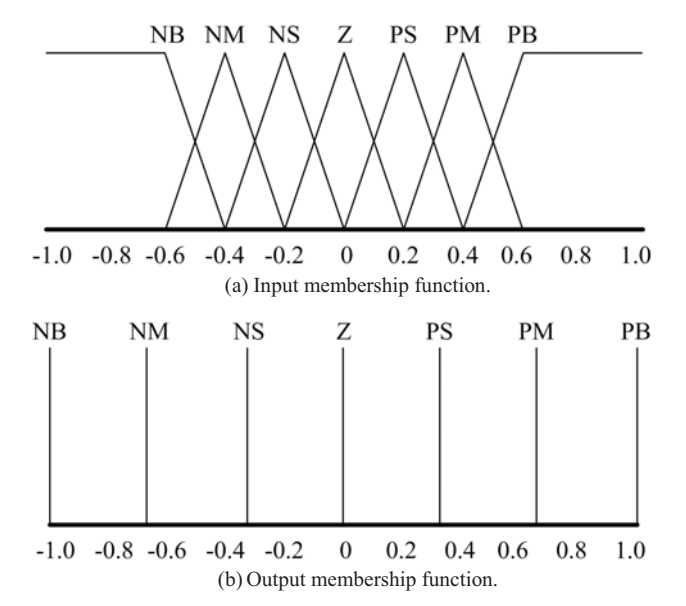


Fig. 2. Block diagram of fuzzy logic control.



eė	NB	NM	NS	Z	PS	PM	РВ
NB	PB	PB	PB	PB	PB	PB	PM
МИ	PB	PB	PB	PM	PM	PM	PM
NS	PM	PM	PM	PS	PS	Z	Z
Z	PB	PM	PS	Z	NS	NM	NB
PS	Z	Z	NS	NS	NM	NM	NM
PM	NM	NM	NM	NM	NB	NB	NB
РВ	NM	NB	NB	NB	NB	NB	NB
(c) Rule base.							

Fig. 3. Rule base and membership functions.

$$y_{\rm T} = \frac{1}{2} C_{\rm Bus} v_{\rm Bus}^2 + \frac{1}{2} C_{\rm SC} v_{\rm SC}^2 \tag{4}$$

The dc bus capacitive energy $y_{\rm Bus}$ is given versus $p_{\rm FCo}$, p_{SCo} , and p_{Load} by the following differential equation:

$$\dot{y}_{\text{Bus}} = p_{\text{FCo}} + p_{\text{SCo}} - p_{\text{Load}} \tag{5}$$

where,
$$p_{\text{FCo}} = p_{\text{FC}} - r_{\text{FC}} \left(\frac{p_{\text{FC}}}{v_{\text{FC}}}\right)^2, \quad p_{\text{SCo}} = p_{\text{SC}} - r_{\text{SC}} \left(\frac{p_{\text{SC}}}{v_{\text{SC}}}\right)^2 \quad \text{where,}$$

$$p_{\text{Load}} = \sqrt{\frac{2y_{\text{Bus}}}{C_{\text{Bus}}}} \cdot i_{\text{Load}}, \quad p_{\text{SC}} = \sqrt{\frac{2y_{\text{SC}}}{C_{\text{SC}}}} \cdot i_{\text{SC}} \quad (6)$$

$$In this case, \quad p_{\text{SCMax}} = \frac{v_{\text{SC}}^2}{4r_{\text{SC}}}, \quad p_{\text{FCMax}} = \frac{v_{\text{FC}}^2}{4r_{\text{FC}}}$$

$$In this case, \quad p_{\text{SCMax}} = \frac{v_{\text{FC}}^2}{4r_{\text{FC}}}$$

III. CONTROL OF A HYBRID POWER SOURCE

A. Control Algorithm

In the proposed system depicted in Fig. 1, there are two voltage variables or two energy variables to be regulated [3]:

- the dc bus energy y_{Bus} is the most important variable.
- the supercapacitor storage energy y_{SC} is of secondary importance.

Therefore, based on the previous literature referenced above, we propose to utilize the supercapacitors, the fastest energy source of the proposed system, to supply the energy for the dc bus [3]. Hence, the FC (as the slowest dynamic device) functions to supply the energy to both the dc bus capacitor C_{Bus} and the supercapacitors $C_{\rm SC}$ to keep them charged.

The flat output [7], [8] $y = [y_1, y_2]^T$, control variable u = $[u_1, u_2]^T$, and state variable $\mathbf{x} = [x_1, x_2]^T$ are defined as:

$$\mathbf{y} = \begin{bmatrix} y_{\text{Bus}} \\ y_{\text{T}} \end{bmatrix}, \quad \mathbf{u} = \begin{bmatrix} p_{\text{SCREF}} \\ p_{\text{FCREF}} \end{bmatrix}, \quad \mathbf{x} = \begin{bmatrix} v_{\text{Bus}} \\ v_{\text{SC}} \end{bmatrix}$$
 (7)

From (3) and (4), the state variables x can be written

$$x_{\rm l} = \sqrt{\frac{2y_{\rm l}}{C_{\rm Bus}}} = \varphi_{\rm l}(y_{\rm l}), \tag{8}$$

$$x_2 = \sqrt{\frac{2(y_2 - y_1)}{C_{SC}}} = \varphi_2(y_1, y_2)$$
 (9)

From (5) and (6), the control variables u can be calculated from the flat output v and its time derivatives (inverse dynamics):

$$u_{1} = 2p_{\text{SCMax}} \cdot \left[1 - \sqrt{1 - \left(\frac{\dot{y}_{1} + \sqrt{\frac{2y_{1}}{C_{\text{Bus}}}} \cdot i_{\text{Load}} - p_{\text{FCo}}}{p_{\text{SCMax}}} \right)} \right]$$
$$= \psi_{1}(y_{1}, \dot{y}_{1}) = p_{\text{SCREF}}$$

$$u_{2} = 2p_{\text{FCMax}} \cdot \left[1 - \sqrt{1 - \left(\frac{\dot{y}_{2} + \sqrt{\frac{2y_{1}}{C_{\text{Bus}}}} \cdot i_{\text{Load}}}{p_{\text{FCMax}}} \right)} \right]$$

$$= \psi_{2}(y_{1}, \dot{y}_{2}) = p_{\text{FCREF}}$$

$$(10)$$

$$= \psi_{2}(y_{1}, \dot{y}_{2}) = p_{\text{FCREF}}$$

$$p_{\text{SCMax}} = \frac{v_{\text{SC}}^2}{4r_{\text{SC}}}, \quad p_{\text{FCMax}} = \frac{v_{\text{FC}}^2}{4r_{\text{FC}}}$$
 (12)

In this case, p_{SCMax} and p_{FCMax} are the limited

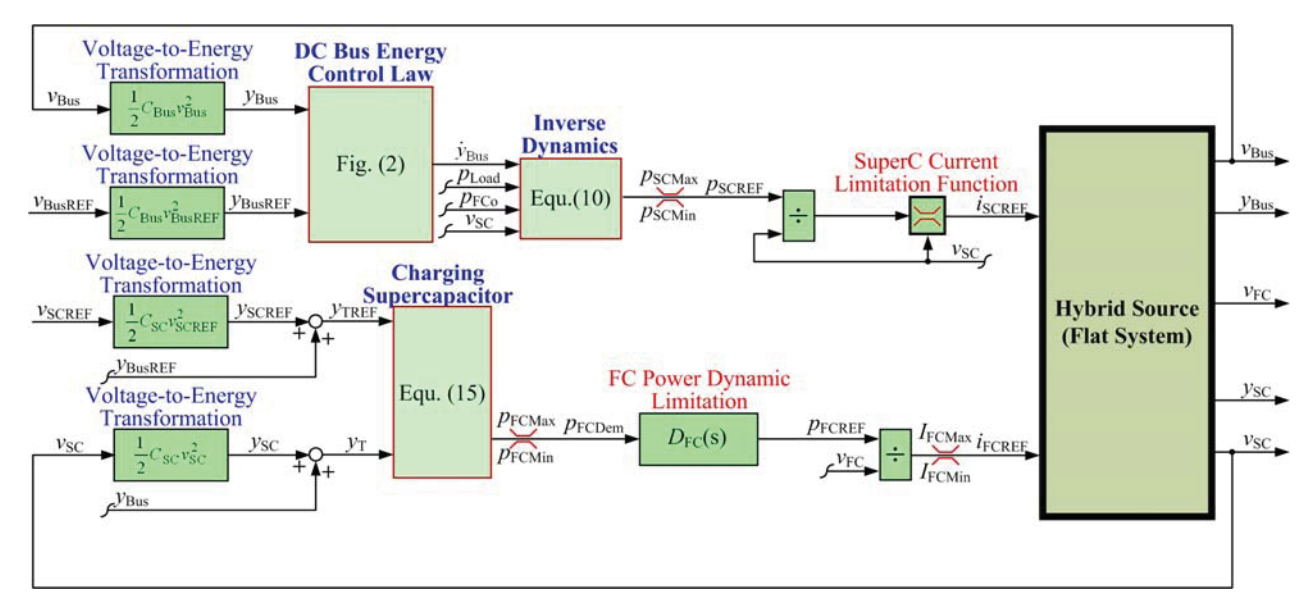


Fig. 4. Control structure of FC/supercapacitor hybrid source.

maximum power of the supercapacitor and FC sources, respectively.

Thus, it is apparent that $x_1 = \varphi_1(y_1)$, $x_2 = \varphi_2(y_1, y_2)$, $u_1 = \psi_1(y_1, \dot{y}_1)$, and $u_2 = \psi_2(y_1, \dot{y}_2)$. Consequently the proposed reduced order system can be considered as a flat system.

B. DC Bus Energy Regulation Based on Fuzzy Logic

Fuzzy logic controller (FLC) can be decomposed of three data processing parts; fuzzification, rule evaluation (inference engine), and defuzzification. The controller is based on fuzzy reasoning mapping between real world information and numerical information. As shown in many applications [9], [10]. Mamdani inference method is the most commonly used inference technique. However, it requires a high performance in computation process since the centroids of membership functions must be obtained. In contrast, Takagi-Sugeno (T-S) with singleton output provides faster evaluation time which could be effectively used in various works [11], [12]. It is also appropriated for real-time applications which need high speed computing hardware such as DSP card or dSPACE. The control objective is to regulate the dc bus voltage level (v_{Bus}). The controller contains Takagi-Sugeno inference engine and two fuzzy inputs: energy error $e_1 (= y_{1REF} - y_1)$ and differential energy error \dot{e}_1 which would be carefully adjusted by proportional gain $(K_{\rm P})$ and derivative gain $(K_{\rm D})$, respectively. In addition, the fuzzy output level could be set by the proportional gain (K_0) as shown in Fig. 2.

Triangular and trapezoidal membership functions are chosen for both two fuzzy inputs as shown in Fig. 3(a). There are seven membership functions for each input comprising of *NB* (Negative Big), *NM* (Negative Medium), *NS* (Negative Small), *Z* (Zero), *PB* (Positive Big), *PM* (Positive Medium) and *PS* (Positive Small). For singleton output membership function, zero-order Sugeno

model is applied where the membership functions are symmetrically set as follows; NB = -1, NM = -0.66, NS = -0.33, Z = 0, PB = 1, PM = 0.66, PS = 0.33, as shown in Fig. 3(b).

For the rule base, expert perception, experimental approach and trial and error technique were employed for defining the relationships between inputs and output. The data representation was in the form of IF-THEN rule as shown in following example.

IF
$$(e_{1i})$$
 is NS and \dot{e}_{1i} is NS THEN $(z_i$: output) is NB.

From Fig. 3(c), the total number of rule base is therefore equal to 49 rules. To obtain the output of controller, centre of gravity method for singletons (COGS) is utilized as:

$$U = \frac{\sum_{i=1}^{N} w_i z_i}{\sum_{i=1}^{N} w_i}$$

$$(13)$$

where the weights (w_i) can be retrieved from

$$w_i = \min(e_{1i}, \dot{e}_{1i}) \tag{14}$$

C. Charging Supercapacitor

For supercapacitor energy regulation, the desired reference for the total energy is represented by y_{2REF} (= y_{TREF}). Because the supercapacitor has an enormous energy storage capacity, and because the supercapacitor energy is defined as a slower dynamic variable than the dc bus energy variable, the total energy control law is defined as [13], [14]:

$$(\dot{y}_2 - \dot{y}_{2REF}) + K_{21}(y_2 - y_{2REF}) = 0$$
 (15)



Fig. 5. Test bench system of the renewable energy power plant.

The multivariable control of the FC/supercapacitor hybrid power source detailed above is portrayed in Fig. 4. The dc-bus energy control law generates a supercapacitor power reference p_{SCREF} . This signal is then divided by the measured supercapacitor voltage v_{SC} and limited to maintain supercapacitor voltage within an interval $[V_{\text{SCMin}}, V_{\text{SCMax}}]$ by limiting a supercapacitor charging current or discharging current, as presented in the block "SuperC Current Limitation Function" [3]. This results in supercapacitor current reference i_{SCREF} . For the supercapacitor energy control law, it generates the FC power demand p_{FCDem} . It must be limited in slope, which enables the safe operation of the FC with respect to the dynamic constraints that are associated with the FC stack. To obtain a natural linear function, a second-order delay (filter) $D_{FC}(s)$ is chosen for the limited FC power dynamics as [15]:

$$D_{FC}(s) = \frac{p_{FCREF}(s)}{p_{FCDem}(s)} = \frac{1}{\left(\frac{s}{\omega_{n1}}\right)^2 + \frac{2\zeta_1}{\omega_{n1}}s + 1}$$
(16)

where ω_{n1} and ζ_1 are the regulation parameters.

IV. EXPERIMENTAL VALIDATION

A. Platform Description

To authenticate the proposed control algorithm and control laws, a small-scale test bench of the hybrid system was implemented in our laboratory, as presented in Figs. 5, 6 and 7. The FC system used in this effort was a PEMFC system (1.2 kW, 46 A; Ballard Power Systems Company). The supercapacitor module (100 F, 32 V; Maxwell Technologies Company) was obtained by means of 12 BCAP1200 cells (1200 F; 2.7 V) connected in series. The FC converter (1.2 kW) and the supercapacitor converter (4 kW) (refer to Fig. 1) were both realized in the laboratory, see Table I.

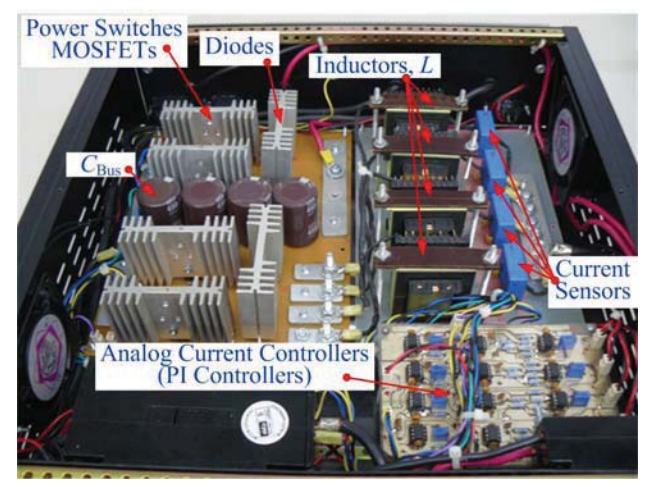


Fig. 6. Implemented fuel cell converter 1,200 W.

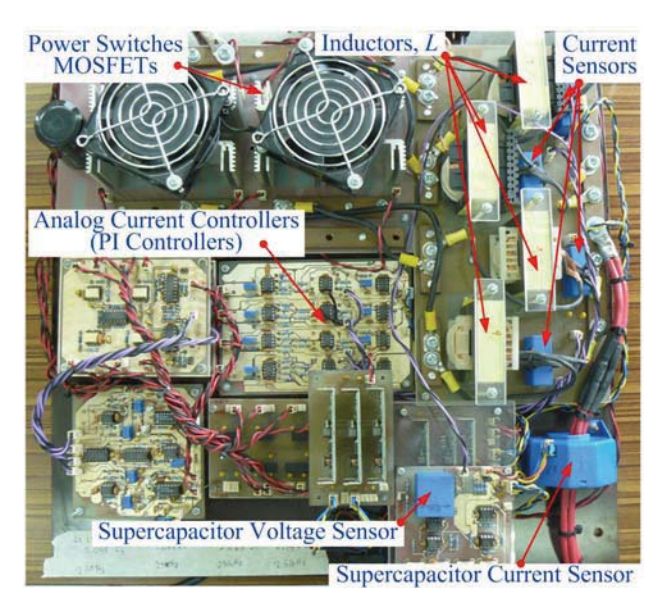


Fig. 7. Implemented supercapacitor converter 3,000 W.

TABLE I
CONVERTER PARAMETERS AND SEMICONDUCTOR DEVICES

Fuel Cell Converter: Inductors $L_{\rm F1} = L_{\rm F2} = L_{\rm F3} = L_{\rm F4}$ 396 μ H MOSFETs $S_{\rm F1} = S_{\rm F2} = S_{\rm F3} = S_{\rm F4}$ IRFP264N: 250 V, 38 A Diodes $D_{\rm F1} = D_{\rm F2} = D_{\rm F3} = D_{\rm F4}$ RURG3020: 200 V, 30 A Supercapacitor Converter: Inductors $L_{\rm C1} = L_{\rm C2} = L_{\rm C3} = L_{\rm C4}$ 150 μ H MOSFETs $S_{\rm C1} = S_{\rm C2} = S_{\rm C3} = S_{\rm C4}$ IRFP264N: 250 V, 38 A $= S_{\rm C1} = S_{\rm C2} = S_{\rm C3} = S_{\rm C4}$

B. Control Description

Measurements of the FC current i_{FC} , the supercapacitor current i_{SC} , the load current i_{Load} , the dc bus voltage v_{Bus} , the FC voltage v_{FC} , and the supercapacitor voltage v_{SC} were carried out by means of zero-flux Hall effect sensors.

TABLE II
DC-BUS ENERGY CONTROL LOOP PARAMETERS

$v_{ m BusREF}$	60	V
$C_{ m Bus}$	12,200	μF
$K_{ m P}$	0.15	
K_{D}	0.15	
K_{O}	-200	
$r_{\rm SC}$	0.01	Ω
$P_{ m SCMax}$	+3,750	W
$P_{\rm SCMin}$	-3,750	W
$V_{ m SCMax}$	32	V
$V_{ m SCMin}$	15	V
$I_{ m SCRated}$	150	A

TABLE III
CHARGING SUPERCAPACITOR CONTROL LOOP PARAMETERS

$v_{ m SCREF}$	25	V	
$C_{ m SC}$	100	F	
K_{21}	0.1		
$r_{ m FC}$	0.1	Ω	
$P_{ m FCMax}$	500	W	
$P_{ m FCMin}$	0	W	
I_{FCMax} (Rated)	46	A	
$I_{ m FCMin}$	0	A	
ζ_1	1		
ω_{nl}	0.4	rad·s⁻¹	

The FC and supercapacitor current regulation loops were realized using analog circuits to function at a high bandwidth. Parameters associated with the dc-bus energy regulation loop and the charging supercapacitor regulation loop can be seen in Tables II and III, respectively. The FC power dynamic delay is shown in Table III. This value has been experimentally determined as having the highest power slope of our FC system, where no fuel starvation occurs [16]. It must be noted that, for the small-test bench, the FC maximum power p_{FCMax} was set at 500 W; in fact, the rated FC power considered here is 1200 W. Moreover, these two energy control loops, which generated current references i_{FCREF} and i_{SCREF} , were implemented in the real-time card dSPACE DS1104 usingMATLAB-Simulink at a sampling frequency of 25 kHz.

C. Experimental Results

The studied dc bus of 60 V is only connected to an electronic load. Waveforms obtained during the large load cycle are presented in Fig. 8. The data show the dc bus voltage, the fuel cell voltage, the load power, the supercapacitor power, the fuel cell power, the supercapacitor current, the fuel cell current, and the supercapacitor voltage (or the supercapacitor SOC). In the initial state, the load power is zero, and the storage device is fully charge, i.e., $v_{SC} = 25$ V; as a result, both the fuel cell and supercapacitor powers are zero. At t = 10 s, the load power steps to the final constant power of around 700 W (positive load power transition). The

following observations are made:

- The supercapacitor supplies most of the 700 W power that is required during the transient step load.
- Concurrently, the fuel cell power increases with limited dynamics (refer to equation (16)) to a maximum power of 500 W.
- The input from the supercapacitor, which supplies most of the transient power that is required during the stepped load, slowly decreases and the unit remains in a discharge state after the load step because the steady-state load power (approximately 700 W) is greater than the main power supplied by the fuel cell.

At t = 40 s, the supercapacitor voltage is equal to 20 V. As a result, the supercapacitor supplies its stored energy y_{SC} to the dc bus. This energy $y_{\text{SC}_\text{Supply}}$ is estimated to be:

$$y_{\text{SC_Supply}} = \frac{1}{2} \cdot C_{\text{SC}} \cdot v_{\text{SC}}^2 (t = 10s) - \frac{1}{2} \cdot C_{\text{SC}} \cdot v_{\text{SC}}^2 (t = 40s)$$

= 11.25 kJ.

The load power is reduced from the high constant power of 700 W to zero (negative load power transition). As a result, the supercapacitor changes from discharging to charging and demonstrates the following three phases:

- First, the fuel cell still supply its constant maximum power to drive the load and to charge the supercapacitor.
- Second, at t = 55 s, the supercapacitor is nearly fully charged, i.e., $v_{SC} = 23.5$ V. As a result, the fuel cell power is reduced with limited power dynamics.
- Third, at t = 86 s, the supercapacitor is fully charged, i.e., $v_{SC} = v_{SCREF} = 25$ V. After slowly decreasing, the fuel cell and supercapacitor powers are zero.

It is evident that the dc bus voltage waveform is stable during the large load cycle, which is critically important when employing supercapacitors to improve the dynamic performance of the whole system using the proposed control law.

To demonstrate dynamic regulation of the dc-bus energy (voltage) of the fuzzy logic controller (refer to Fig. 2), the oscilloscope waveforms in Fig. 9 show the dc bus voltage dynamics (representing the flat output y_1) to the large load power demanded (disturbance) from 0 to 600 W and 0 to 750 W, whereas the dc bus was loaded with an electronic load. The oscilloscope screens show the dc-bus voltage (the state variable x_1 , representing the flat output y_1), the supercapacitor voltage (the state variable x_2), the load power, and the supercapacitor power (the control input variable u_1).

The fuel cell power dynamics were purposely limited (see Fig. 8), forcing the supercapacitor to supply the transient load power demand. The proposed fuzzy logic controller show good stability and optimum response (no oscillation and short settling time) of the dc-bus voltage regulation to its desired reference of 60 V.

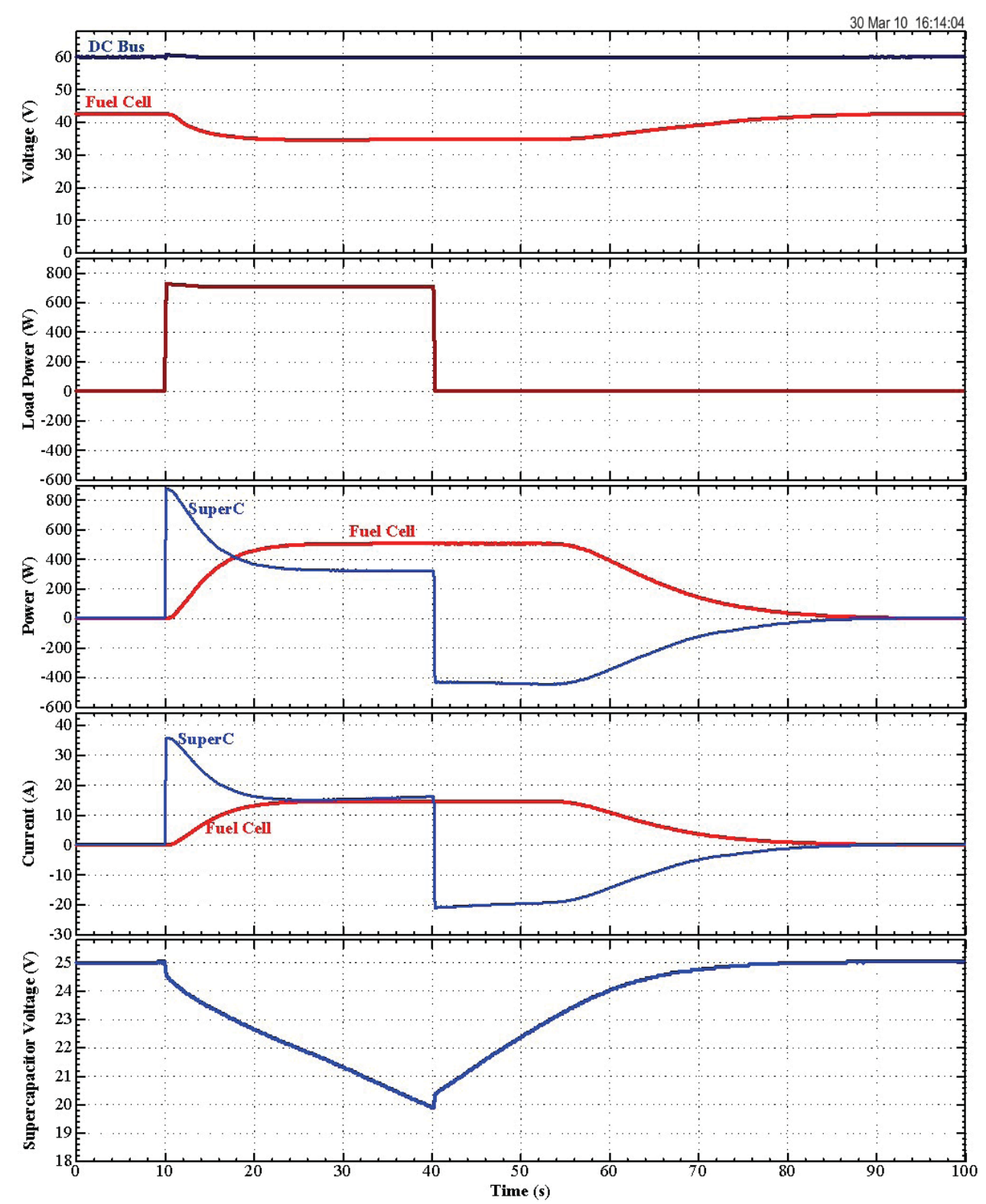
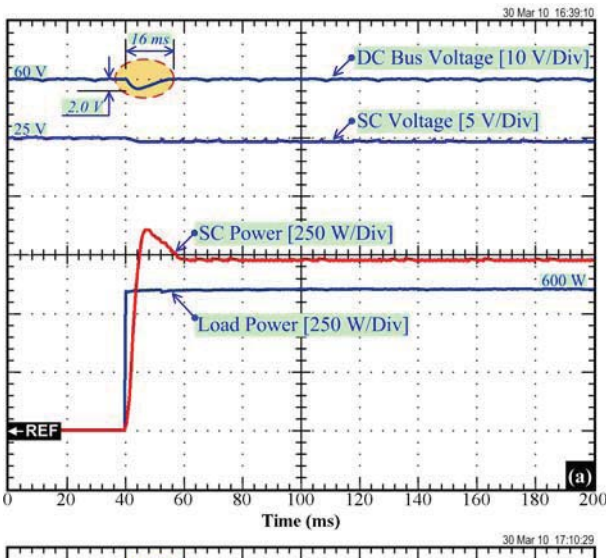


Fig. 8. Experimental results of hybrid source during load cycle.

Note that there are some losses (static and dynamic losses) in the supercapacitor converter (see Fig. 1), because the implemented converters are hard-switching converters, then, the power difference between the supercapacitor and the load powers (for example, during 60 to 200 ms) can be observed. To improve the converter

efficiency, soft-switching converters may be effective solutions for future work.



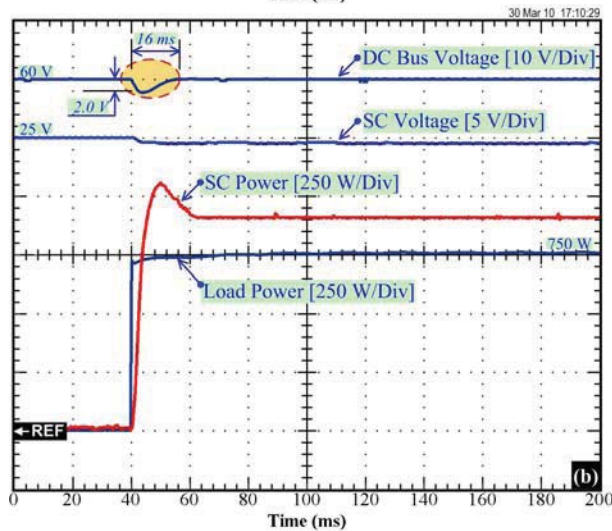


Fig. 9. Experimental results of dynamic characteristic of the hybrid source during a step load from. (a) 0 to 600 W, (b) 0 to 750 W.

V. CONCLUSION

This paper has proposed the control of the dc link stabilization for power plant supplied by an FC main source and a supercapacitor supplementary source. The main contribution of this paper is the implementation and experimental authentication of the T-S fuzzy control based-on the differential flatness approach for the dc link stabilization (energy balance) for dc distributed generation systems. Experimental verification with a small-scale power plant (Nexa Ballard FC power generator: 1.2 kW, 46A; Maxwell supercapacitor storage device: 100 F, 32 V) has demonstrated the excellent performance of the whole system, and has validated the proposed energy management principle.

ACKNOWLEDGMENT

The authors would like to thank S. Lekapat, who is in charge of the process of the "Franco-Thai on Higher Education and Research Joint Project year: 2009-2010" and of the research funding for this paper.

REFERENCES

- [1] P. Corbo, F. Migliardini, and O. Veneri, "Experimental analysis of a 20 kWe PEM fuel cell system in dynamic conditions representative of automotive applications," *Energy Convers Manage.*, vol. 49, pp. 2688–2697, 2008.
- [2] P. Thounthong, S. Raël, and B. Davat, "Control algorithm of fuel cell and batteries for distributed generation system," *IEEE Trans. Energy Convers.*, vol. 23, no. 1, pp. 148–155, Jan. 2008.
- [3] P. Thounthong, S. Raël, and B. Davat, "Analysis of supercapacitor as second source based on fuel cell power generation," *IEEE Trans. Energy Convers.*, vol. 24, no. 1, pp. 247–255, Mar. 2009.
- [4] A. Gensior, H. Sira-Ramirez, J. Rudolph, H. Guldner, "On some nonlinear current controllers for three-phase boost rectifiers," *IEEE Trans. Ind. Electron.*, vol. 56, no. 2, pp. 360–370, Feb. 2009.
- [5] A. Payman, S. Pierfederici, and F. Meibody-Tabar, "Energy control of supercapacitor/fuel cell hybrid power source," *Energy Convers. Manage.*, vol. 49, no. 6, pp. 1637–1644, Jun. 2008.
- [6] P. Thounthong, B. Davat, S. Raël, and P. Sethakul, "Fuel cell high-power applications," *IEEE Ind. Electron. Mag.*, vol. 3, no. 1, pp. 32–46, March 2009.
- [7] M. Fliess, J. Lévine, Ph. Martin, and P. Rouchon, "Flatness and defect of nonlinear systems: Introductory theory and examples," *Int. J. Contr.*, vol. 61, no. 6, pp. 1327–1361, 1995.
- [8] M. Fliess, J. Lévine, Ph. Martin, and P. Rouchon, "A lie-bäcklund approach to equivalence and flatness of nonlinear systems," *IEEE Trans. Automat. Contr.*, vol. 44, no. 5, pp. 922–937, May 1999.
- [9] S.M. Gadoue, D. Giaouris, and J.W. Finch, "MRAS sensorless vector control of an induction motor using new sliding-mode and fuzzy-logic adaptation mechanisms," *IEEE Trans. Energy Convers.*, vol. 25, no. 2, pp. 394– 402, June 2010.
- [10] S.M. Muyeen, R. Takahashi, T. Muata, and J. Tamura, "Integration of an Energy Capacitor System With a Variable-Speed Wind Generator," *IEEE Trans. Energy Convers.*, vol. 24, no. 3, pp. 740–749, Sep. 2009.
- [11] V. Galdi, A. Piccolo, and P. Siano, "Designing an adaptive fuzzy controller for maximum wind energy extraction," *IEEE Trans. Energy Convers.*, vol. 23, no. 2, pp. 559-569, June 2008.
- [12] C.S. Chiu, "T-S Fuzzy Maximum Power Point Tracking Control of Solar Power Generation Systems," *IEEE Trans. Energy Convers.*, vol. 25, no. 4, pp. 1123-1132, 2010.
- [13] M. A. Danzer, J. Wilhelm, H. Aschemann, and E. P. Hofer, "Modelbased control of cathode pressure and oxygen excess ratio of a PEM fuel cell system," *J. Power Sources*, vol. 176, no. 2, pp. 515–522, 2008.
- [14] E. Song, A. F. Lynch, and V. Dinavahi. "Experimental validation of nonlinear control for a voltage source converter," *IEEE Trans. Control System Technology*, vol. 17, no. 5, pp. 1135–1144, Sept. 2009.
- [15] P. Thounthong, S. Raël, and B. Davat, "Analysis of differential flatness-based control for a fuel cell hybrid power source," *IEEE Trans. Energy Convers.*, vol. 25, no. 3, pp. 909–920, Sep. 2010.
- [16] P. Thounthong, B. Davat, S. Raël, and P. Sethakul, "Fuel starvation: analysis of a PEM fuel cell system," *IEEE Ind. Appl. Mag.*, vol. 15, no. 4, pp. 52–59, July-Aug. 2009.

Model Based-Energy Control of a Solar Power Plant With a Supercapacitor for Grid-Independent Applications

Phatiphat Thounthong, Member, IEEE

Abstract—This paper proposes a design for a renewable-energy hybrid power plant that is fed by a photovoltaic (PV) source with a supercapacitor (SC) storage device and is suitable for distributed generation applications. The PV array is used as the main generator, and the SC functions as an auxiliary source for supplying the (transient and steady-state) power deficiency of the PV array. For high-power applications, four-phase parallel boost converters and four-phase parallel bidirectional converters are implemented as a PV converter and a storage device, respectively. A reduced-order mathematical model of the PV and SC converters is described for the control of the power plant. Using a nonlinear approach based on the flatness property, we propose a simple solution to the dynamic, stabilization, and robustness problems in the hybrid power system. This is the key innovative contribution of this research paper. We analyze a prototype small-scale power plant composed of a 0.8-kW PV array and a 100-F SC module. The experimental results authenticate the excellent control algorithm during load cycles.

Index Terms—Converters, flatness, hybrid source, nonlinear control, photovoltaic (PV), supercapacitor (SC).

I. INTRODUCTION

URRENTLY, renewable energy is receiving greater attention as a sustainable alternative to more traditional energy sources. One of these environmentally friendly energy sources is solar energy; however, there are still some severe concerns about several sources of renewable energy and their implementation, e.g., 1) capital costs and 2) their intermittent power production, called the "intermittency problem." The intermittency problem of solar energy is that solar panels cannot produce power steadily because their power production rates change with seasons, months, days, hours, etc. If there is no sunlight, no electricity will be produced from the photovoltaic (PV) cell.

To overcome the intermittency problem, a storage medium or electrical energy carrier [a battery or a supercapacitor (SC)]

Manuscript received March 24, 2011; revised July 6, 2011; accepted September 6, 2011. Date of publication October 10, 2011; date of current version November 23, 2011. This work was supported in part by the research program in cooperation with the Thai–French Innovation Institute, King Mongkut's University of Technology North Bangkok with the Institut National Polytechnique de Lorraine, Nancy University, under the "Franco-Thai on Higher Education and Research Joint Project year: 2009–2010," and in part by the Thailand Research Fund under Grant MRG5380261. Paper no. TEC-00153-2011.

The author is with the Department of Teacher Training in Electrical Engineering (TE), King Mongkut's University of Technology North Bangkok (KMUTNB), Bangkok 10800, Thailand (e-mail: phatiphat.thounthong@ensem.inpl-nancy.fr).

Color versions of one or more of the figures in this paper are available online at http://ieeexplore.ieee.org.

Digital Object Identifier 10.1109/TEC.2011.2168400

is needed. An SC storage device is preferable due to its high power density, fast energy sourcing, and long lifetime [1]. In the near future, the utility power system will be supplied on a large scale by solar energy sources and storage device(s) in a *hybrid energy system* to increase the reliability and effectiveness of the individual components [2].

The dynamics, robustness, and stability of the operation of hybrid power plants are of particular interest. In this work, a hybrid power generation system is proposed and it consists of the following main components: a PV source and an SC as a highpower density device. The most popular way to control power converters in the industry today is with a linear control structure [3], [4]. The design of the linear proportional-integral (PI) controller usually proceeds by incorporating the switching mode controller into the plant (converter). Later averaging and linearization enables the employ of the Laplace transform [5], [6]. The PI controller may then be designed for a certain phase margin, normally around 30-60°. Because the switching model of the hybrid power plant (power electronic converters) is nonlinear, it is natural to apply model-based nonlinear control strategies that directly compensate for system nonlinearity without requiring a linear approximation [7].

Currently, many modeling and linear or nonlinear control aspects, including classical state-space or transfer approaches [8], [9], self-tuning methods or sliding mode control [10], the exact linearization technique [11], adaptive control [12], or fuzzy logic-based control [13], have been extensively studied for nonlinear power electronic applications. Flatness-based control has recently been studied in many applications because it is appropriate for robustness, predictive control, trajectory planning, and constraint handling. Based on the flatness approach, the state feedback can be chosen in such a way that the closed-loop dynamic behavior is linear [14]. Flat systems are linearizable in the quasi-static state feedback. When used for tracking, quasi-static state feedback is very useful.

The flatness theory was introduced by Fliess *et al.* [14] in 1995. Recently, these ideas have been used in a variety of nonlinear systems across the various engineering disciplines, including the following applications: the control of an inverted pendulum and a vertical take-off and landing aircraft [15]; the process of a stirred tank chemical reactor [16]; the control of vehicle steering [17]; the control of a high-speed linear axis driven by pneumatic muscle actuators [18]; the control of cathode pressure and the oxygen excess ratio of a proton exchange membrane (PEM) fuel cell system [19]; the steering control of a two-level quantum system [20]; the reactive power and the

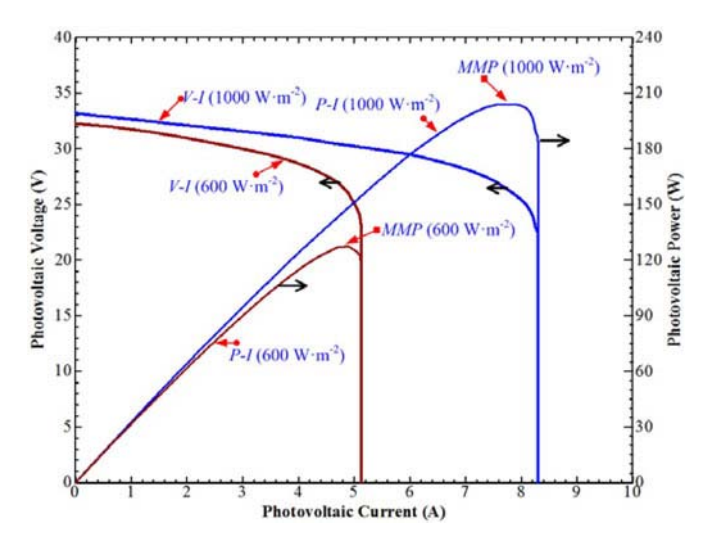


Fig. 1. Power versus current characteristics and voltage versus current characteristics based on a 200-W PV module by the Ekarat Solar at fixed ambient temperature and variable insolation (1000 and 600 $W\cdot m^{-2}$).

dc voltage tracking control of a three-phase voltage source converter [21]; the control of open-channel flow in an irrigation canal [22]; and the current control for three-phase three-wire boost converters [23].

We now study an uncomplicated design of a control system of the PV/SC power plant based upon the physical structure of the model. The main contribution of this paper is to present the differential flatness-based control approach of a solar power generation system with an SC storage device. In particular, we do not restrict ourselves to linear control techniques at an equilibrium point. This is the novel work in this domain. The remaining of the paper is structured as follows: the next section describes the hybrid energy system and the power plant model that is studied in this work. In Section III, the proposed energy management algorithm is presented. In Section IV, a proof of the flat system consisting of the solar energy power plant, the control laws, and the system stability is presented. In Section V, the test bench results for the proposed system are presented. Finally, this paper ends with concluding remarks for further study in Section VI.

II. POWER SOURCE CHARACTERISTICS

A. Photovoltaic

The PV effect is a basic physical process through which solar energy is converted directly into electrical energy. The physics of a PV cell, or solar cell, is similar to the classical p–n junction diode. The V–I and P–I characteristic curves of the PV model used in this study (200-W PV Module by the Ekarat Solar Company) under different irradiances (at 25 °C) are given in Fig. 1. As shown in Fig. 1, the higher the irradiance, the larger the short-circuit current $I_{\rm SC}$ and the open-circuit voltage $V_{\rm OC}$. As a result, the output PV power will also be larger.

Remark 1: PV power systems require some specific estimation algorithms to deliver the maximum power point (MPP) [24], [25]. Because of the typical low-efficiency characteristics of PV panels, it is very important to deliver the maximum instantaneous power from these energy sources to the load with

minimum power conversion for space or terrestrial applications. Temperature also plays an important role in the PV array performance. The lower the temperature, the higher the maximum power and the larger the open-circuit voltage. It is obligatory to use dc/dc or dc/ac converters with effective MPP tracking (MPPT) techniques [26].

B. Supercapacitor

The SC (or double-layer capacitor or ultracapacitor) is an emerging technology in the field of energy-storage systems. Recent breakthroughs in construction methods aimed at maximizing rated capacitance have provided tremendous increases in the energy-storage capabilities of the double-layer capacitor [27]. With a time constant (the product of equivalent series resistance (ESR) and capacitance) of 0.001–2 s for an SC, the stored energy can be extracted at a very high rate because the ESR inside an SC is very small [28]. In contrast, the same-sized battery will not be able to supply the necessary energy in the same time period because of the higher time constant of the battery [27], [29].

The operating voltage of an SC changes linearly with time during constant current operation so that the state-of-charge can be precisely estimated. In addition, the highly reversible electrostatic charge storage mechanism in SCs does not lead to the volume changes observed in batteries with electrochemical transformations of active masses. This volume change usually limits the lifetime cycle of batteries to several hundred cycles, whereas SCs have demonstrated from hundreds of thousands to many millions of full charge/discharge cycles [30], [31].

The SC bank is always connected to the dc bus by means of a two-quadrant dc/dc converter (bidirectional converter). Fig. 2 presents the transient response of an SC converter interfacing between the dc bus and the SC bank (SAFT SC module: 292 F, 30 V) [32]. The initial voltage of the SC bank is 30 V. The SC current set-point (reference) is Ch2 and the measured SC current is Ch4. The dynamic response of the SC auxiliary source is very fast and can discharge from 0 to 50 A in 0.4 ms.

Remark 2: To operate the SC module, its module voltage is limited to an interval [$V_{\rm SCMin}$, $V_{\rm SCMax}$]. The higher $V_{\rm SCMax}$ value of this interval corresponds to the rated voltage of the storage device. In general, the lower $V_{\rm SCMin}$ value is chosen as $V_{\rm SCMax}/2$, where the remaining energy in the SC bank is only 25% and the SC discharge becomes ineffective [32].

III. SOLAR POWER PLANT

A. Structure of the Studied Power Converters

Low-voltage, high-current (power) converters are needed because of the electrical characteristics of the PV cell and the SC bank. A classical boost converter is often used as a PV converter [33], and a classical two-quadrant (bidirectional) converter is often used as an SC or battery converter [27]. However, the classical converters will be limited when the power increases or at higher step-up ratios. Therefore, the use of parallel power converters (multiphase converters in parallel) with interleaving may offer better performance in terms of dynamics [34], because

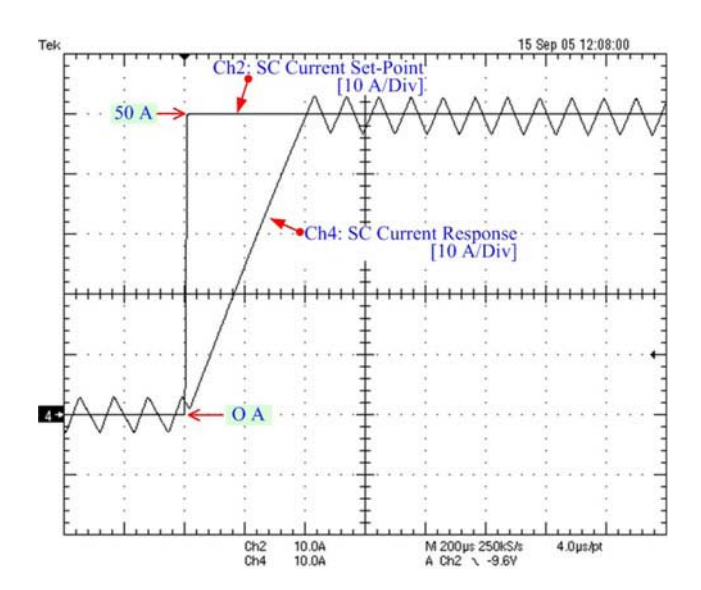


Fig. 2. SC current response to a 0–50 A step (discharging).

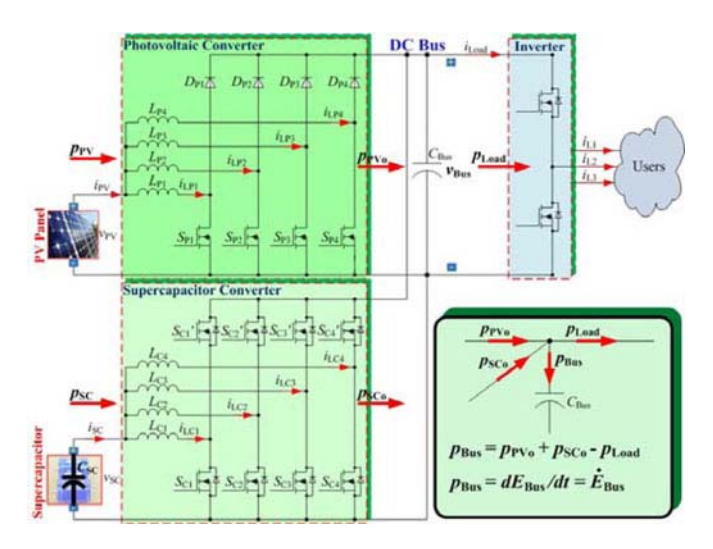


Fig. 3. Proposed circuit diagram of the distributed generation system supplied by a PV and SC, where $p_{\rm Load}$ (= $\nu_{\rm Bus}$ \times $i_{\rm Load}$), $\nu_{\rm Bus}$, and $i_{\rm Load}$ are the load power, the dc-bus voltage, and the dc-bus load current, respectively. $p_{\rm PV}$ (= $\nu_{\rm PV}$ \times $i_{\rm PV}$), $\nu_{\rm PV}$, and $i_{\rm PV}$ are the PV power, voltage, and current, respectively. $p_{\rm SC}$ (= $\nu_{\rm SC}$ \times $i_{\rm SC}$), $\nu_{\rm SC}$, and $i_{\rm SC}$ are the SC power, voltage, and current, respectively. $p_{\rm PVo}$ and $p_{\rm SCo}$ are the output powers to the dc link from the converters of the PV array and the SC, respectively.

of smaller inductor and capacitor sizes. Next, Fig. 3 depicts the proposed hybrid source structure. The PV converter combines four-phase parallel boost converters with interleaving, and the SC converter employs four-phase parallel bidirectional converters with interleaving.

B. Power Regulation Loops of the Proposed Power Plant

For safety and dynamics, the PV and SC converters are primarily controlled by inner current regulation loops (or power regulation loops), as depicted in Figs. 4 and 5 [32]. These power control loops are supplied by two reference signals: the SC power reference $p_{\rm SCREF}$ and the PV power reference $p_{\rm PVREF}$, generated by the control laws presented later.

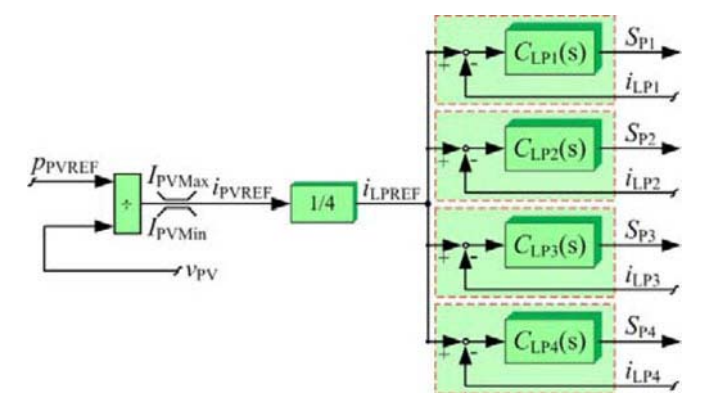


Fig. 4. Photovoltaic power control loop.

For the PV power control, a PV power reference $p_{\rm PVREF}$ is divided by the measured photovoltaic voltage $v_{\rm PV}$, resulting in a PV current reference $i_{\rm PVREF}$. For the SC power control loop, an SC power reference $p_{\rm SCREF}$ is divided by the measured SC voltage $v_{\rm SC}$ and limited to maintain the SC voltage within an interval $[V_{\rm SCMin}, V_{\rm SCMax}]$, according to Remark 2 by the SC current limitation function. This calculation results in an SC current reference $i_{\rm SCREF}$ [32].

C. Mathematical Model of the Power Plant

We assume that the PV and SC currents follow their reference values perfectly. Consequently,

$$i_{\text{PV}} = i_{\text{PVREF}} = \frac{p_{\text{PV}}}{v_{\text{PV}}} = \frac{p_{\text{PVREF}}}{v_{\text{PV}}}$$
 (1)

$$i_{\rm SC} = i_{\rm SCREF} = \frac{p_{\rm SC}}{v_{\rm SC}} = \frac{p_{\rm SCREF}}{v_{\rm SC}}.$$
 (2)

We only consider static losses in these converters, and $r_{\rm PV}$ and $r_{\rm SC}$ represent static losses in the PV and SC converters, respectively. Now, the PV array and the SC storage device function as controlled current sources connected with the equivalent series resistance that is called a reduced-order model [35].

The dc-bus capacitive energy E_{Bus} and the supercapacitive energy E_{SC} can be written as

$$E_{\rm Bus} = \frac{1}{2} C_{\rm Bus} v_{\rm Bus}^2 \tag{3}$$

$$E_{\rm SC} = \frac{1}{2} C_{\rm SC} v_{\rm SC}^2.$$
 (4)

The total electrostatic energy E_T stored in the dc-bus capacitor $C_{\rm Bus}$ and the SC $C_{\rm SC}$ can also be written as

$$E_T = \frac{1}{2}C_{\text{Bus}}v_{\text{Bus}}^2 + \frac{1}{2}C_{\text{SC}}v_{\text{SC}}^2.$$
 (5)

Note that the total electrostatic energy E_T is nearly equal to the energy stored in the SC $C_{\rm SC}$ because the SC size $C_{\rm SC}$ is much greater than the dc-bus capacitor size $C_{\rm Bus}$.

The derivative of dc-bus capacitive energy $\dot{E}_{\rm Bus}$ is given versus $p_{\rm PVo}, p_{\rm SCo}$, and $p_{\rm Load}$ by the following differential equation:

$$\dot{E}_{\rm Bus} = p_{\rm PVo} + p_{\rm SCo} - p_{\rm Load} \tag{6}$$

where

$$p_{\text{PVo}} = p_{\text{PV}} - r_{\text{PV}} \left(\frac{p_{\text{PV}}}{v_{\text{PV}}}\right)^2 \tag{7}$$

$$p_{\rm SCo} = p_{\rm SC} - r_{\rm SC} \left(\frac{p_{\rm SC}}{v_{\rm SC}}\right)^2 \tag{8}$$

$$p_{\text{Load}} = v_{\text{Bus}} \cdot i_{\text{Load}}.$$
 (9)

Note that the derivative of dc-bus capacitive energy $dE_{\rm bus}/dt$ is the power $p_{\rm Bus}$ flows into the dc-bus capacitor. It means that $p_{\rm Bus}$ is equal to $dE_{\rm bus}/dt$ ($\dot{E}_{\rm Bus}$)(see Fig. 3).

IV. CONTROL OF A POWER PLANT

A. Energy Balance

In the proposed system depicted in Fig. 3, there are two voltage variables (or two energy variables) to be regulated.

- 1) The dc-bus energy $E_{\rm Bus}$ is the most important variable.
- 2) The SC storage energy $E_{\rm SC}$ is the next most important.

Therefore, we propose utilizing SCs, which are the fastest energy source in the proposed system, to supply the energy for the dc bus [32]. In fact, we plan to functionalize the PV array by supplying energy only for charging the SC $C_{\rm SC}$. However, during charging, the energy from the PV cell flows through the dc bus to the SC bank. For this reason, the PV array is mathematically operated to supply energy for both the dc-bus capacitor $C_{\rm Bus}$ and the SC $C_{\rm SC}$ to keep them charged.

B. Differential Flatness Property

Let us first reveal a physical property, used to establish the system flatness [14], [15], [36], that will be the main concept for our reference generations. The flat outputs y, the control input variables u, and the state variables x are defined as

$$\mathbf{y} = \begin{bmatrix} y_1 \\ y_2 \end{bmatrix} = \begin{bmatrix} E_{\text{Bus}} \\ E_{\text{T}} \end{bmatrix}, \qquad \mathbf{u} = \begin{bmatrix} u_1 \\ u_2 \end{bmatrix} = \begin{bmatrix} p_{\text{SCREF}} \\ p_{\text{PVDEM}} \end{bmatrix},$$
$$\mathbf{x} = \begin{bmatrix} x_1 \\ x_2 \end{bmatrix} = \begin{bmatrix} v_{\text{Bus}} \\ v_{\text{SC}} \end{bmatrix}$$
(10)

where p_{PVDEM} is the PV power demand. It will be generated by the outer controller. This signal will send to an MPPT in order to saturate the PV maximum power. It becomes the PV power reference p_{PVREF} , presented hereafter.

From (3) and (6), the dc-bus voltage $v_{\rm Bus}$ (defined as a state variable x_1) and the SC power (defined as a control input variable u_1) can be expressed as an algebraic function

$$x_1 = \sqrt{\frac{2y_1}{C_{\text{Bus}}}} = \varphi_1(y_1) \tag{11}$$

$$u_1 = 2p_{\text{SCLim}}$$

$$\cdot \left[1 - \sqrt{1 - \left(\frac{\dot{y}_1 + i_{\text{Load}} \cdot \varphi_1 \left(y_1 \right) - p_{\text{PVo}}}{p_{\text{SCLim}}} \right)} \right]$$

$$= \psi_1 \left(y_1, \dot{y}_1 \right) = p_{\text{SCREF}} \tag{12}$$

$$p_{\text{SCLim}} = \frac{v_{\text{SC}}^2}{4r_{\text{SC}}} \tag{13}$$

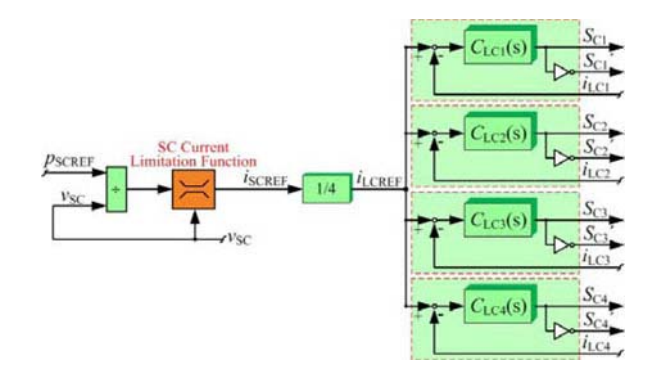


Fig. 5. SC power control loop.

where $p_{\rm SCLim}$ is the limited maximum power from the SC converter.

From (5) and (6), the SC voltage v_{SC} (defined as a state variable x_2) and the PV power p_{PV} (defined as a control input variable u_2) can be expressed as an algebraic function

$$x_2 = \sqrt{\frac{2(y_2 - y_1)}{C_{SC}}} = \varphi_2(y_1, y_2)$$
 (14)

$$u_2 = 2p_{\mathrm{PVLim}} \cdot \left[1 - \sqrt{1 - \left(\frac{\dot{y}_2 + i_{\mathrm{Load}} \cdot \varphi_1\left(y_1\right)}{p_{\mathrm{PVLim}}}\right)}\right]$$

$$=\psi_2(y_1,\dot{y}_2)=p_{\text{PVDEM}} \tag{15}$$

$$p_{\text{PVLim}} = \frac{v_{\text{PV}}^2}{4r_{\text{PV}}} \tag{16}$$

where P_{PVLim} is the limited maximum power from the PV converter.

It is evident that $x_1 = \varphi_1(y_1)$, $x_2 = \varphi_2(y_1, y_2)$, $u_1 = \psi_1(y_1, \dot{y}_1)$, and $u_2 = \psi_2(y_1, \dot{y}_2)$. Consequently, the PV/SC power plant can be considered a flat system [36].

C. Control Law and Stability

Let us now focus our attention on the feedback design to track a dc-bus energy reference trajectory y_{1REF} and a total energy reference y_{2REF} . We aim to design a feedback law such that the tracking error $(y_1-y_{1REF}, y_2-y_{2REF})$ asymptotically vanishes. Thus, the relative degree of the first input v_1 and the second input v_2 is 1. The proposed control laws [37] are

$$(\dot{y}_1 - \dot{y}_{1REF}) + K_{11} (y_1 - y_{1REF}) = 0$$
 (17)

$$(\dot{y}_2 - \dot{y}_{2REF}) + K_{21} (y_2 - y_{2REF}) = 0.$$
 (18)

Because the SC can store enormous amount of energy, and the supercapacitive energy is defined as a slower dynamic variable than the dc-bus energy variable, in order to compensate for nonideal effects, an integral term is added to the control law (17). This yields

$$v_{1} = \dot{y}_{1} = \dot{y}_{1REF} + K_{11} (y_{1REF} - y_{1})$$

$$+ K_{12} \int_{0}^{t} (y_{1REF} - y_{1}) d\tau$$
(19)

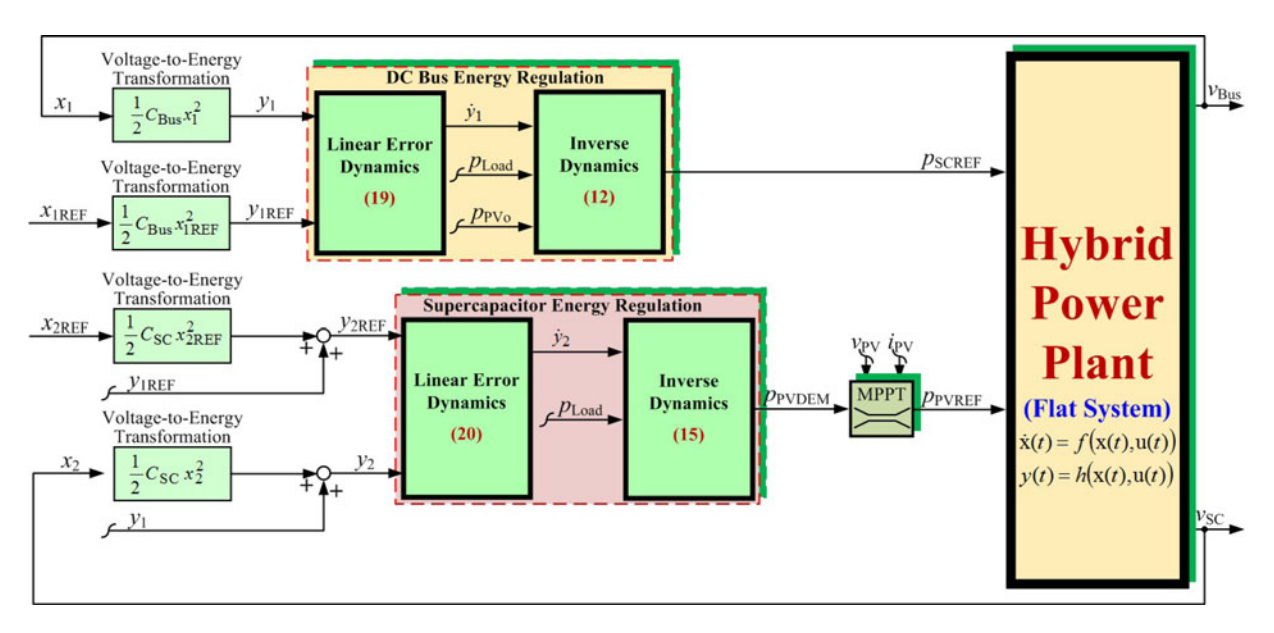


Fig. 6. Multivariable control of a PV/SC hybrid power plant based on a differential flatness approach.

$$v_2 = \dot{y}_2 = \dot{y}_{2REF} + K_{21} (y_{2REF} - y_2).$$
 (20)

From (19), if we define $e_1 = y_1 - y_{1REF}$, $K_{11} = 2\zeta\omega_n$, and $K_{12} = \omega_n^2$, we obtain

$$\ddot{e}_1 + 2\zeta\omega_n \cdot \dot{e}_1 + \omega_n^2 \cdot e_1 = 0. \tag{21}$$

Substituting the expression for \dot{y}_1 from (19) into (12) gives the equation for the closed-loop static state feedback SC power. From (20), if we define $e_2 = y_2 - y_{2\text{REF}}$, $K_{21} = 1/\tau_S$, we obtain

$$\tau_{\rm S} \cdot \dot{e}_2 + e_2 = 0. \tag{22}$$

Substituting the expression for \dot{y}_2 from (20) into (15) gives the equation for the closed-loop static state feedback PV power. It is clear that the control system is asymptotically stable for K_{11} , $K_{12}>0$, and $K_{21}>0$. However, based on the power electronic constant switching frequency ω_S and cascade control structure, the outer control loop (here the dc-bus energy control) must operate at a cutoff frequency $\omega_E << \omega_C << \omega_S$, where ω_C is a cutoff frequency of the SC power loop. Once the flat outputs are stabilized, the whole system becomes exponentially stable because all of the variables of the system are expressed in terms of the flat outputs [36].

In Fig. 6, the proposed control algorithm of the renewable energy power plant, as detailed earlier, is depicted. The dc-bus energy control law generates an SC power reference $p_{\rm SCREF}$ ($=u_1$, refer to (12)). The total energy control law (or the SC energy control) generates a PV power demand $p_{\rm PVDEM}$ ($=u_2$, refer to (15)). This signal must be saturated at the maximum power point by MPPT according to *Remark 1*.

It should be concluded here that, in this application, the PV does not always operate at its MPP in a stand-alone (grid-independent) scenario, as depicted in Fig. 6.

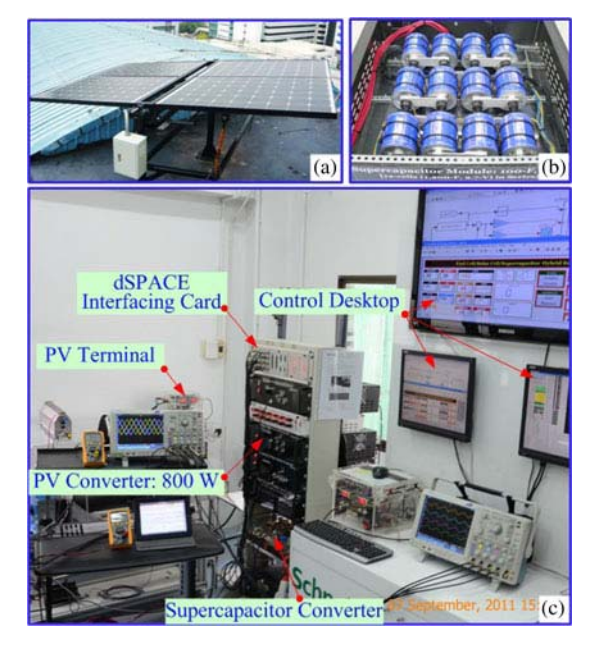


Fig. 7. Photograph of a test bench power plant. (a) solar cell panels, (b) SC bank, and (c) test bench.

V. PERFORMANCE VALIDATIONS

A. Power Plant Description for a Test Bench

To validate the performance of the modeling and control system, the small-scale test bench of the hybrid power plant was implemented in our laboratory, as presented in Fig. 7. The prototype 0.8-kW PV converter and the 2-kW SC converter (refer to Fig. 3) were implemented in the laboratory. Specifications of the PV module and storage device are detailed in Table I.

TABLE I
SPECIFICATIONS OF PHOTOVOLTAIC SOURCE AND STORAGE DEVICE

Photovoltaic Array (by Ekarat Solar Co	mpany):	
Number of Panels in Parallel	4	
Panel Open Circuit Voltage	33.5	V
Panel Rated Voltage	26	V
Panel Rated Current	7.7	Α
Panel Rated Power	200	W
Array Rated Power	800	W
Supercapacitor Bank (by Maxwell Tec	hnologies	Comp
(Cell Model: BCAP1200)		
Number of Cells in Series	12	
Cell Capacity	1,200	F
Cell Maximum Voltage	2.7	V
Bank Capacity (C_{SC})	100	F
	32	12000

TABLE II
DC-BUS ENERGY CONTROL LOOP PARAMETERS

v_{BusREF}	60	V
C_{Bus}	12200	μ F
K_{11}	450	rad·s ⁻¹ rad ² ·s ⁻²
K_{12}	22,500	rad ² ·s ⁻²
$r_{\rm PV}$	0.12	Ω
$r_{\rm SC}$	0.10	Ω
V_{SCMax}	32	V
$V_{\rm SCMin}$	15	V
I_{SCRated}	150	A

TABLE III
SUPERCAPACITIVE ENERGY CONTROL LOOP PARAMETERS

v_{SCREF}	25	V	
$C_{\rm SC}$	100	F	
K_{21}	0.1	$W \cdot J^{-1}$	
p _{PVMax} (Rated)	800	W	
I _{PVMax} (Rated)	30.8	A	
I_{PVMin}	0	A	
ΔI_{PV}	0.1	A	
Δt	6	ms	

B. Control Description

The parameters associated with the dc-bus energy regulation loop are summarized in Table II. The parameters associated with the SC energy regulation loop are detailed in Table III. For the low-scale test bench, the dc-bus voltage reference $v_{\rm BusREF}$ (= $x_{\rm 1REF}$) was set to 60 V and the SC voltage reference $v_{\rm SCREF}$ (= $x_{\rm 2REF}$) was set to 25 V (the nominal value of the SC bank).

The constant switching frequency ω_S of the PV and SC converters was 25 kHz (157 080 rad·s⁻¹). The nonlinear controller gains used were $K_{11}=450~{\rm rad\cdot s^{-1}}$ and $K_{12}=22~500~{\rm rad^2\cdot s^{-2}}$ so that the system damping ratio ζ was equal to 1.5 and the natural frequency ω_n was equal to 150 rad·s⁻¹. As a result, the cutoff frequency ω_E of the closed-loop dc-bus energy was equal to 60 rad·s⁻¹. This value was lower than the cutoff frequency ω_C of the SC power loop of 450 rad·s⁻¹ (equivalent to a first-order delay with a time constant T_C of 2.2 ms) so that the system was asymptotically stable [36]. The controller gain of the closed-loop supercapacitive energy was $K_{21}=0.1~{\rm W\cdot J^{-1}}$ so that the cutoff frequency $\omega_{\rm SC}$ of the closed-loop supercapacitive

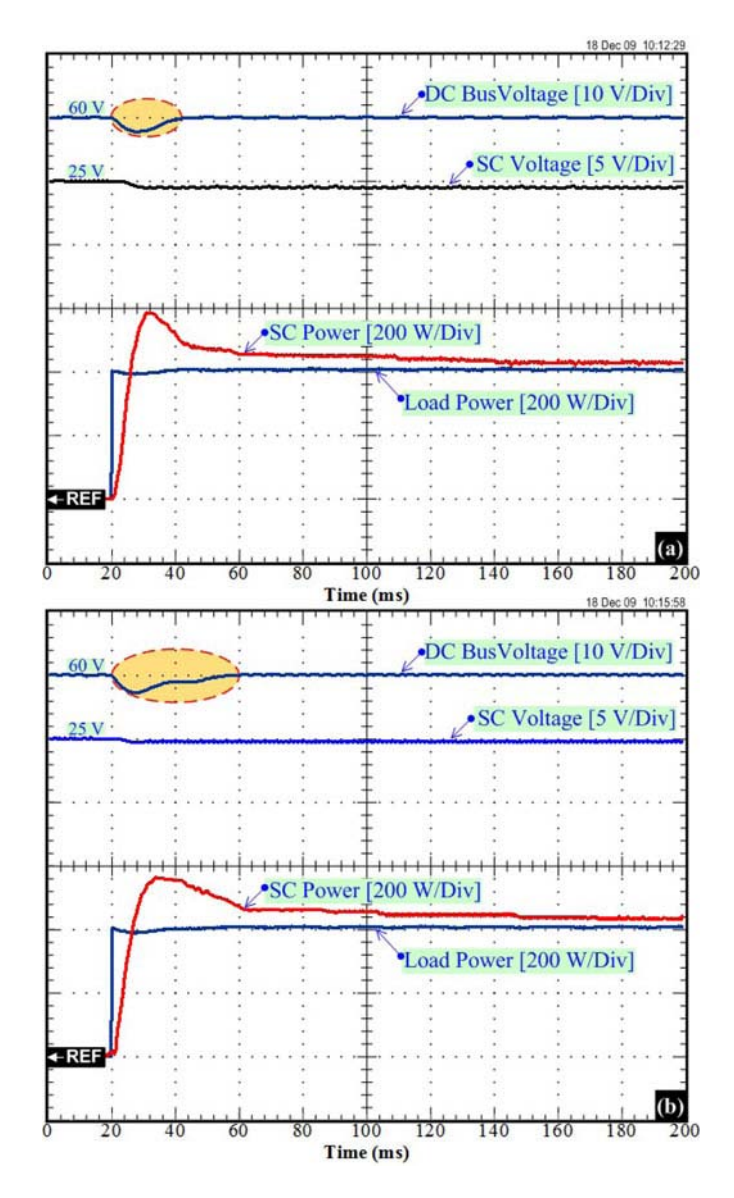


Fig. 8. Comparison of the dc-link stabilization of the power plant during a large load step. (a) Exact model ($r_{\rm PV}=0.12~\Omega, r_{\rm SC}=0.10~\Omega$). (b) Error model (robustness) ($r_{\rm PV}=0.001~\Omega, r_{\rm SC}=0.001~\Omega$).

energy was equal to $0.1 \text{ rad} \cdot \text{s}^{-1}$ in which $\omega_{\text{SC}} \ll \omega_E$, in order to guarantee the asymptotic stability of the whole system.

The PV and SC current regulation loops and the electronic protections were realized by analog circuits. The two energy-control loops, which generate current references $i_{\rm PVREF}$ and $i_{\rm SCREF}$, were implemented in the real-time card dSPACE DS1104 platform (see Fig. 7) using the fourth-order *Runge–Kutta* integration algorithm and a sampling time of 80 μ s within the mathematical environment of MATLAB–Simulink.

C. Experimental Results

Because flatness-based control is model based, it may have some sensitivity to error in model parameters. To authenticate its robustness, the flatness-based control was tested with the exact model parameters ($r_{\rm PV}=0.12~\Omega$ and $r_{\rm SC}=0.10~\Omega$) and the erroneous parameters case ($r_{\rm PV}=0.001~\Omega$ and $r_{\rm SC}=0.001~\Omega$)

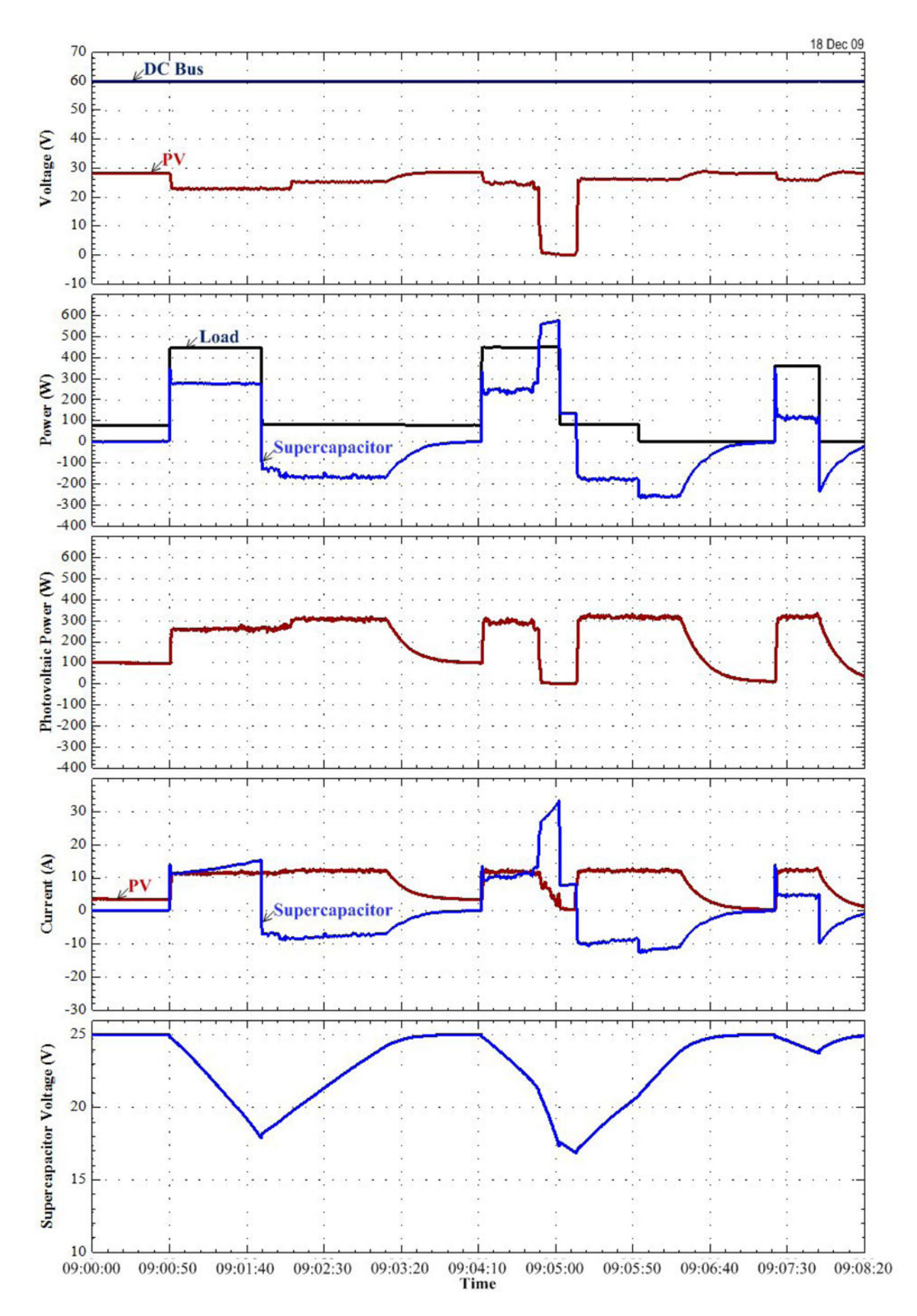


Fig. 9. Experimental results: power plant response during load cycles.

 $0.001~\Omega$). For the sake of the dc-bus voltage stabilization and robust control system, the oscilloscope waveforms in Fig. 8 show the comparison (robustness) between the accurate parameters and the error parameters. It portrays the dynamic characteristics that are obtained during the large load step. It shows the dc-bus voltage, the load power (disturbance), the SC power, and the SC voltage. The initial state is in no-load power, the SC storage device is full of charge, i.e., the SC voltage = 25 V ($v_{\rm SCREF}$ = 25 V), and the dc-bus voltage is regulated at 60 V ($\nu_{\rm BusREF}$ = 60 V); as a result, the PV and SC powers are zero. At t =20 ms, the large load power steps from 0 W to a constant value of 400 W (positive transition). Because during the transient state the PV power is limited by MPPT estimation, the SC supplies the transient load power demand. One can scrutinize the similar waveforms in Fig. 8(a) and (b). The dc-bus voltage (dc-link stabilization) is minimally influenced by the large load power step. Clearly, the performance of the control system is minimally affected by the model parameter error considered. Experimental testing demonstrates that errors in these parameters had relatively little effect on regulation performance, and we conclude that the nonlinear differential flatness-based approach provides a robust controller in this application.

Finally, for the sake of the dc-bus voltage stabilization and load profile (load cycles), Fig. 9 presents waveforms that are obtained during the load cycles measured on December 18, 2009, at an ambient temperature of around 25 °C. In Fig. 9, the dc-bus voltage, the PV voltage, the load power (disturbance), the SC power, the PV power, the SC current, the PV current, and the SC voltage are shown. In the initial state, the small load power is equal to 100 W, and the storage device is full of charge, i.e., $v_{\rm SC}=25$ V; as a result, the SC power is zero and the PV source supplies 100 W of power for the load. At 09:00:50, the load power steps to the final constant power of around 450 W (positive load power transition). We observe the following phenomena.

- 1) The SC supplies most of the transient power that is required during the step load.
- 2) Simultaneously, the PV power increases to an MPP of around 250 W, which is limited by the MPPT.
- Concurrently, the SC remains in a discharge state after the load step because the steady-state load power (approximately 450 W) is greater than the power supplied by the PV array.

After that phase, one can again observe that the power plant is always energy balanced ($p_{\text{Load}}(t) = p_{\text{PV}}(t) + p_{\text{SC}}(t)$) by the proposed original control algorithm. One can observe that the dc-bus voltage waveform is asymptotically stable during the large load cycles, which is of major importance when employing SC to improve the dynamic performance of the whole system using the proposed control law.

VI. CONCLUSION AND FURTHER WORKS

The main contribution of this paper is to model and control a PV/SC hybrid power plant. The prototype power plant is composed of a PV array (800 W, Ekarat Solar) and an SC module (100 F, 32 V, Maxwell Technologies). A compact topology,

suitable for high-power applications, is proposed. Its working principle, analysis, and design procedure are presented. The PV array is the main source, and the SC functions as a storage device (or an auxiliary source) to compensate for the uncertainties of the PV source in the steady state and the transient state. An SC can advance the load, following the characteristics of the main sources, by providing a stronger power response to changes in the system load. Adding energy storage to the distributed power systems improves power quality and efficiency.

Using the nonlinear control approach based on the flatness property, we propose a simple solution to the dynamic, stabilization, and robustness problems in the nonlinear power electronic system. And also, there are no operating points comparable with a classical linear control. This is a novel concept for this kind of application. However, the proposed control law needs a load current measurement to estimate the load power. For future work, a load observer will be used to avoid a measurement of a load current, as was explored in [23].

ACKNOWLEDGMENT

The author would like to thank Dr. P. Sethakul (KMUTNB), Dr. S. Pierfederici, and Dr. B. Davat (Nancy University) for their valuable comments and suggestions about power electronics and control.

REFERENCES

- Y. Cheng, "Assessments of energy capacity and energy losses of supercapacitors in fast charging-discharging cycles," *IEEE Trans. Energy Con*vers., vol. 25, no. 1, pp. 253–261, Mar. 2010.
- [2] M. Liserre, T. Sauter, and J. Y. Hung, "Future energy systems: Integrating renewable energy sources into the smart power grid through industrial electronics," *IEEE Ind. Electron. Mag.*, vol. 4, no. 1, pp. 18–37, Mar. 2010.
- [3] A. El Aroudi and M. Orabi, "Stabilizing technique for AC–DC boost PFC converter based on time delay feedback," *IEEE Trans. Circuits Syst. II, Exp. Briefs*, vol. 57, no. 1, pp. 56–60, Jan. 2010.
- [4] Suroso and T. Noguchi, "A new three-level current-source PWM inverter and its application for grid connected power conditioner," *Energy Con*vers. Manage., vol. 51, no. 7, pp. 1491–1499, Jul. 2010.
- [5] Y. A. Hajizadeh, M. A. Golkar, and A. Feliachi, "Voltage control and active power management of hybrid fuel-cell/energy-storage power conversion system under unbalanced voltage sag conditions," *IEEE Trans. Energy Convers.*, vol. 25, no. 4, pp. 1195–1208, Dec. 2010.
- [6] L. Ming, C. K. Tse, H. H. C. Iu, M. Xikui, and M. Orabi, "Unified equivalent modeling for stability analysis of parallel-connected DC/DC converters," *IEEE Trans. Circuits Syst. II, Exp. Briefs*, vol. 57, no. 11, pp. 898–902, Nov. 2010.
- [7] P. Thounthong, S. Pierfederici, J.-P. Martin, M. Hinaje, and B. Davat, "Modeling and control of fuel cell/supercapacitor hybrid source based on differential flatness control," *IEEE Trans. Veh. Technol.*, vol. 59, no. 6, pp. 2700–2710, Jul. 2010.
- [8] N. Gyawali and Y. Ohsawa, "Integrating fuel cell/electrolyzer/ultracapacitor system into a stand-alone microhydro plant," *IEEE Trans. Energy Convers.*, vol. 25, no. 4, pp. 1092–1101, Dec. 2010.
- [9] K. Acharya, S. K. Mazumder, and I. Basu, "Reaching criterion of a three-phase voltage-source inverter operating with passive and nonlinear loads and its impact on global stability," *IEEE Trans. Ind. Electron.*, vol. 55, no. 4, pp. 1795–1812, Apr. 2008.
- [10] X. Yu and O. Kaynak, "Sliding-mode control with soft computing: A survey,," *IEEE Trans. Ind. Electron.*, vol. 56, no. 9, pp. 3275–3285, Sep. 2009.
- [11] W. K. Na and B. Gou, "Feedback-linearization-based nonlinear control for PEM fuel cells," *IEEE Trans. Energy Convers.*, vol. 23, no. 1, pp. 179– 190, Mar. 2008.

- [12] F. Jadot, F. Malrait, J. Moreno-Valenzuela, and R. Sepulchre, "Adaptive regulation of vector-controlled induction motors," *IEEE Trans. Control Syst. Technol.*, vol. 17, no. 3, pp. 646–657, May 2009.
- [13] C.-S. Chiu, "T-S fuzzy maximum power point tracking control of solar power generation systems," *IEEE Trans. Energy Convers.*, vol. 25, no. 4, pp. 1123–1132, Dec. 2010.
- [14] M. Fliess, J. Lévine, Ph. Martin, and P. Rouchon, "Flatness and defect of nonlinear systems: Introductory theory and examples," *Int. J. Contr.*, vol. 61, no. 6, pp. 1327–1361, 1995.
- [15] M. Fliess, J. Lévine, Ph. Martin, and P. Rouchon, "A Lie–Bäcklund approach to equivalence and flatness of nonlinear systems," *IEEE Trans. Automat. Contr.*, vol. 44, no. 5, pp. 922–937, May 1999.
- [16] M. Guay, "On the linearizability of nonisothermal continuous stirred-tank reactors," *Automatica*, vol. 38, no. 2, pp. 269–278, Feb. 2002.
- [17] J. Villagra, B. A. Novel, H. Mounier, and M. Pengov, "Flatness-based vehicle steering control strategy with SDRE feedback gains tuned via a sensitivity approach," *IEEE Trans. Control Syst. Technol.*, vol. 15, no. 3, pp. 554–564, May 2007.
 [18] H. Aschemann and D. Schindele, "Sliding-mode control of a high-speed
- [18] H. Aschemann and D. Schindele, "Sliding-mode control of a high-speed linear axis driven by pneumatic muscle actuators,," *IEEE Trans. Ind. Electron.*, vol. 55, no. 1, pp. 3855–3864, Nov. 2008.
- [19] M. A. Danzer, J. Wilhelm, H. Aschemann, and E. P. Hofer, "Model-based control of cathode pressure and oxygen excess ratio of a PEM fuel cell system," *J. Power Sources*, vol. 176, no. 2, pp. 515–522, Feb. 2008.
- [20] P. S. P. da Silva and P. Rouchon, "Flatness-based control of a single qubit gate,," *IEEE Trans. Automat. Contr.*, vol. 53, no. 3, pp. 775–779, Apr. 2008.
- [21] E. Song, A. F. Lynch, and V. Dinavahi, "Experimental validation of non-linear control for a voltage source converter," *IEEE Trans. Control Syst. Technol.*, vol. 17, no. 5, pp. 1135–1144, Sep. 2009.
- [22] T. Rabbani, S. Munier, D. Dorchies, P. Malaterre, A. Bayen, and X. Litrico, "Flatness-based control of open-channel flow in an irrigation canal using SCADA," *IEEE Control Syst. Mag.*, vol. 29, no. 5, pp. 22–30, Oct. 2009.
- [23] A. Gensior, H. Sira-Ramirez, J. Rudolph, and H. Guldner, "On some non-linear current controllers for three-phase boost rectifiers,," *IEEE Trans. Ind. Electron.*, vol. 56, no. 2, pp. 360–370, Feb. 2009.
- [24] L. R. Chen, C. H. Tsai, Y. L. Lin, and Y. S. Lai, "A biological swarm chasing algorithm for tracking the PV maximum power point," *IEEE Trans. Energy Convers.*, vol. 25, no. 2, pp. 484–493, Jun. 2010.
- [25] T. L. Gibson and N. A. Kelly, "Solar photovoltaic charging of lithium-ion batteries," J. Power Sources, vol. 195, no. 12, pp. 3928–3932, Jun. 2010.
- [26] O. Lopez, F. D. Freijedo, A. G. Yepes, P. F. Comesana, J. Malvar, R. Teodorescu, and J. Doval-Gandoy, "Eliminating ground current in a transformerless photovoltaic application," *IEEE Trans. Energy Convers.*, vol. 25, no. 1, pp. 140–147, Mar. 2010.
- [27] A. Khaligh and Z. Li, "Battery, ultracapacitor, fuel cell, and hybrid energy storage systems for electric, hybrid electric, fuel cell, and plug-in hybrid electric vehicles: state of the art," *IEEE Trans. Veh. Technol.*, vol. 59, no. 6, pp. 2806–2814, Jul. 2010.
- [28] J. R. Mille, "Introduction to electrochemical capacitor technology," *IEEE Electr. Insulat. Mag. Mille*, vol. 26, no. 4, pp. 40–47, Jul. 2010.

- [29] V. Agarwal, K. Uthaichana, R. A. DeCarlo, and L. H. Tsoukalas, "Development and validation of a battery model useful for discharging and charging power control and lifetime estimation," *IEEE Trans. Energy Convers.*, vol. 25, no. 1, pp. 140–147, Mar. 2010.
- [30] M. Inagaki, H. Konno, and O. Tanaike, "Carbon materials for electrochemical capacitors," *J. Power Sources*, vol. 195, no. 24, pp. 7880–7903, Dec. 2010.
- [31] A. Hammar, P. Venet, R. Lallemand, G. Coquery, and G. Rojat, "Study of accelerated aging of supercapacitors for transport applications," *IEEE Trans. Ind. Electron.*, vol. 57, no. 12, pp. 3972–3979, Dec. 2010.
- [32] P. Thounthong, S. Raël, and B. Davat, "Analysis of supercapacitor as second source based on fuel cell power generation," *IEEE Trans. Energy Convers.*, vol. 24, no. 1, pp. 247–255, Mar. 2009.
- [33] G. Spagnuolo, G. Petrone, S. V. Araujo, C. Cecati, E. Friis-Madsen, E. Gubia, D. Hissel, M. Jasinski, W. Knapp, M. Liserre, P. Rodriguez, R. Teodorescu, and P. Zacharias, "Renewable energy operation and conversion schemes: A summary of discussions during the seminar on renewable energy systems," in *IEEE Ind. Electron. Mag.*, no. 1. vol. 4, Mar. 2010, pp. 38–51.
- [34] P. Thounthong and B. Davat, "Study of a multiphase interleaved stepup converter for fuel cell high power applications,," *Energy Convers. Manage.*, vol. 51, no. 4, pp. 826–832, Apr. 2010.
- [35] S. D. Sudhoff, K. A. Corzine, S. F. Glover, H. J. Hegner, and H. N. Robey, Jr., "DC link stabilized field oriented control of electric propulsion systems," *IEEE Trans. Energy Convers*, vol. 13, no. 1, pp. 27–33, Mar. 1998.
- [36] P. Thounthong, S. Pierfederici, and B. Davat, "Analysis of differential flatness-based control for a fuel cell hybrid power source," *IEEE Trans. Energy Convers.*, vol. 25, no. 3, pp. 909–920, Sep. 2010.
- [37] P. Thounthong and S. Pierfederici, "A new control law based on the differential flatness principle for multiphase interleaved DC–DC converter," *IEEE Trans. Circuits Syst. II, Exp. Briefs*, vol. 57, no. 11, pp. 903–907, Nov. 2010.



Phatiphat Thounthong (M'09) received the B.S. and M.E. degrees in electrical engineering from King Mongkut's Institute of Technology North Bangkok (KMITNB), Bangkok, Thailand, in 1996 and 2001, respectively, and the Ph.D. degree in electrical engineering from the Institut National Polytechnique de Lorraine (INPL)-Nancy University, Nancy-Lorraine, France. in 2005.

He is currently an Associate Professor in the Department of Teacher Training in Electrical Engineering (TE), King Mongkut's University of Technology

North Bangkok (KMUTNB). His current research interests include power electronics, electric drives, and electrical devices (fuel cell, solar cell, wind turbine, batteries, and SC).

A New Control Law Based on the Differential Flatness Principle for Multiphase Interleaved DC–DC Converter

Phatiphat Thounthong, Member, IEEE, and Serge Pierfederici

Abstract—This brief presents an innovative control law for a distributed dc generation supplied by a dc power source, here, a fuel cell (FC) generator. Basically, an FC is always connected with a power-electronic converter. This kind of system is a nonlinear behavior. Classically, to control the voltage, the current, or the power in the converter, a linearized technique is often used to study the stability and to select the controller parameters of the nonlinear converter. In this brief, a nonlinear-control algorithm based on the flatness property of the system is proposed. Flatness provides a convenient framework for meeting a number of performance specifications on the power converter. Utilizing the flatness property, we propose simple solutions to the system performance and stabilization problems. Design controller parameters are autonomous of the operating point. To validate the proposed method, a prototype FC power converter (1.2-kW four-phase boost converters in parallel) is realized in the laboratory. The proposed control law based on the flatness property is implemented by digital estimation in a dSPACE 1104 controller card. Experimental results with a polymer electrolyte membrane FC of 1200 W and 46 A in the laboratory corroborate the excellent control scheme.

Index Terms—Converters, flatness-based control, fuel cells (FCs), interleaved, nonlinear, power control.

I. INTRODUCTION

POLYMER electrolyte membrane fuel cells (PEMFCs) as dc generators have become an overwhelming competitor in the distributed generation due to their insuperable advantages, such as high energy efficiency, near-zero emissions, ease of installation, quiet operation, and fewer moving parts and higher power quality [1], [2].

Manuscript received March 8, 2010; revised May 10, 2010 and July 2, 2010; accepted August 23, 2010. Date of publication November 1, 2010; date of current version November 17, 2010. This work was supported in part by a research program in cooperation with the Thai–French Innovation Institute, King Mongkut's University of Technology North Bangkok (KMUTNB), and the Institut National Polytechnique de Lorraine, Nancy Université, under the Franco-Thai Higher Education and Research Joint Project (2009–2010), by the Faculty of Technical Education under Grant FTE255301, by the Thailand Research Fund under Grant MRG5380261, by the National Research Council of Thailand under Grant NRCT40/2553, and by KMUTNB under Grant KMUTNB2553. This paper was recommended by Associate Editor H. S.-H. Chung.

P. Thounthong is with the Department of Teacher Training in Electrical Engineering and the Renewable Energy Research Centre, King Mongkut's University of Technology North Bangkok, Bangkok 10800, Thailand (e-mail: phtt@kmutnb.ac.th; Phatiphat.Thounthong@ensem.inpl-nancy.fr).

S. Pierfederici is with the Groupe de Recherche en Electrotechnique et Electronique de Nancy, Institut National Polytechnique de Lorraine, Nancy Université, 54510 Nancy, France (e-mail: Serge.Pierfederici@ensem.inpl-nancy.fr).

Digital Object Identifier 10.1109/TCSII.2010.2082830

Parallel dc-dc converters are widely used in high-power applications [2]. They operate under a closed-loop feedback control to regulate the output voltage and enable load sharing. These closed-loop converters are intrinsically nonlinear systems. The common method of controlling dc-dc chopper converters still relies on averaged small-signal models and then facilitating the application of the linear-control theory, such as the proportional-integral (PI) controller [3]. Nonetheless, there are situations where this technique offers a limited performance.

This brief presents a new control law based on the differential flatness theory for nonlinear power-electronic switching applications. Here, only the inner fuel cell (FC) power regulation loop is studied. In this kind of system, the main important specification is that a power dynamic response must follow a power reference as fast as possible. By using the nonlinear flatness property, the power regulation loop will operate at very high dynamics. This brief is organized as follows. Section II shows the differential equations describing the ideal multiphase boost converters with an interleaving switching technique for FC high-power applications. In Section III, the brief of the differential flatness principle is introduced. Section IV discusses the proof of differential flatness of the proposed FC converter models and the control law and stability. Experimental results will authenticate the proposed control system in Section V. A comparative study between the flatness control and a linear PI control will be presented in Section VI. Finally, this brief ends with concluding remarks in Section VII.

II. MULTIPHASE INTERLEAVED BOOST CONVERTER FOR FC HIGH-POWER APPLICATIONS

A. Power Converter

Fundamentally, low-voltage high-current (power) converters are needed because of the FC electrical characteristics [1]. A classical boost converter is frequently selected as an FC converter [2], [4]. However, the classical converters will be limited when the power increases or for higher step-up ratios. In this manner, the utilization of paralleling power converters (multiphase converter in parallel) with an interleaved technique may offer some better performances [2]. As a general rule, the interleaved switching technique is composed of phase shifting the control signals of several converter cells N in parallel [5]. Fig. 1 shows the functional diagram of the proposed multiphase interleaved step-up converter for FC applications.

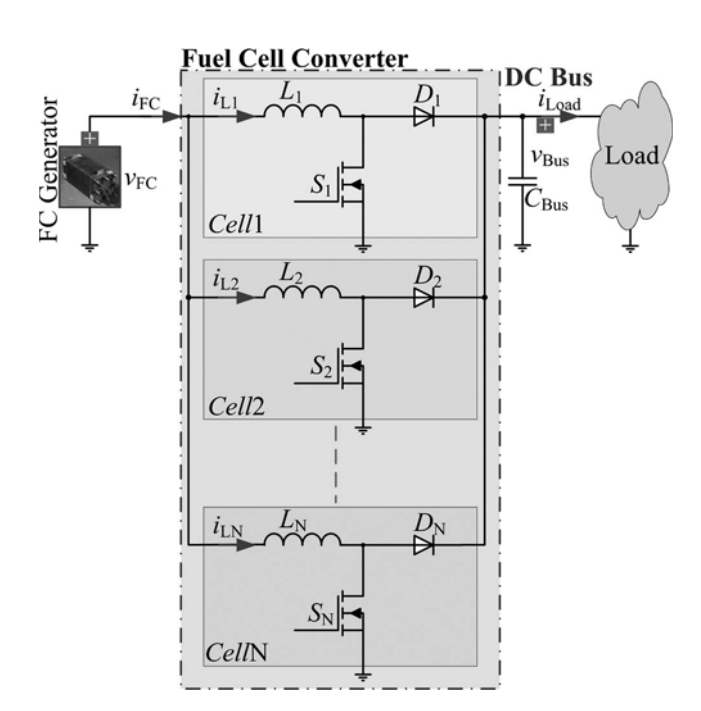


Fig. 1. Multiphase parallel boost converters for FC applications.

B. Boost Converter Average Model

The state equations of the multiphase converters are given as

$$L_K \frac{di_{L_K}}{dt} = v_{FC} - R_{L_K} \cdot i_{L_K} - (1 - d_K) \cdot v_{Bus} \quad (1)$$

$$C_{\text{Bus}} \frac{dv_{\text{Bus}}}{dt} = \sum_{K=1}^{N} (1 - d_K) \cdot i_{L_K} - \frac{v_{\text{Bus}}}{R_{\text{Load}}}$$
 (2)

where the subscript number K = 1, 2, ..., N represents the parameters of each converter module, d is the duty cycle of the pulsewidth modulation (PWM) converter, v_{Bus} is the dc bus voltage, $v_{\rm FC}$ is the FC voltage, $i_{\rm FC}$ is the FC current, i_L is the inductor current, R_{Load} is the equivalent resistance as a load at the dc bus, L is the input inductance, C_{Bus} is the total output capacitance at the dc bus, and R_L is the series resistance of inductor L_K . Note that R_L represents the static losses in each boost converter module.

The power of each cell can be written as

$$p_{L_1} = v_{FC} \cdot i_{L_1}, p_{L_2} = v_{FC} \cdot i_{L_2}, \dots, p_{L_N} = v_{FC} \cdot i_{L_N}$$
 (3)

$$p_{\rm FC} = \sum_{K=1}^{N} v_{\rm FC} \cdot i_{L_K} \tag{4}$$

$$p_{\rm FC} = v_{\rm FC} \cdot i_{\rm FC}.\tag{5}$$

Then, the input power p_L of each cell is given versus $v_{\rm FC}$ and i_L by the following differential equation:

$$\frac{dp_L}{dt} = \frac{d(v_{FC} \cdot i_L)}{dt} = i_L \cdot \frac{dv_{FC}}{dt} + v_{FC} \cdot \frac{di_L}{dt}$$
 (6)

$$\frac{dp_L}{dt} = \frac{d(v_{FC} \cdot i_L)}{dt} = i_L \cdot \frac{dv_{FC}}{dt} + v_{FC} \cdot \frac{di_L}{dt} \qquad (6)$$

$$\frac{dp_L}{dt} = v_{FC} \cdot \frac{di_L}{dt} \Big|_{v_{FC} \approx \text{Constant}}. \qquad (7)$$

III. BRIEF OF THE DIFFERENTIAL FLATNESS PRINCIPLE

Currently, many modeling and linear- or nonlinear-control methods, including classical state-space or transfer approaches [6], self-tuning methods or sliding mode control [7], or fuzzy-

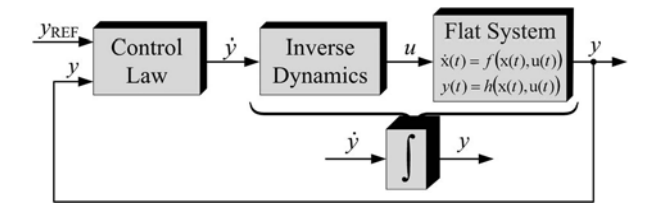


Fig. 2. Concept of the flatness-based control, where y is the output variable, $y_{\rm REF}$ is the output setpoint, and u is the control input variable.

logic-based control [8], [9], have been extensively studied for nonlinear power-electronic applications.

The flatness theory was introduced by Fliess et al. [10] in 1995. Lately, these ideas have been used in a variety of nonlinear systems across the various engineering disciplines, including the following: the control of an inverted pendulum and a vertical takeoff and landing aircraft [10]; the control of cathode pressure and oxygen excess ratio of a PEMFC system [11]; the reactive power and dc voltage tracking control of a three-phase voltage source converter [12]; and the current control for three-phase three-wire boost converters [13]. Since the flatness-based control is model based, one expects it to have some sensitivity to error in model parameters. However, Song et al. [12] have proved that the flatness-based control is robust and provides an improved transient tracking performance relative to a traditional linear-control (PI controller) method.

A nonlinear system is flat [9], [14], [15] if there exists a set of differentially independent variables (equal in number to the number of inputs) such that all state variables x and (control) input variables u can be expressed in terms of those output variables y and a finite number of their time derivatives without integrating differential equations. More specifically, consider the nonlinear dynamic system of the general form, i.e.

$$\begin{vmatrix}
\dot{\mathbf{x}}(t) = f(\mathbf{x}(t), \mathbf{u}(t)) \\
\mathbf{y}(t) = h(\mathbf{x}(t), \mathbf{u}(t))
\end{vmatrix}$$
(8)

where

$$\mathbf{x} = [x_1, x_2, \dots x_n]^T, \qquad \mathbf{x} \in \mathbb{R}^n$$

$$\mathbf{u} = [u_1, u_2, \dots u_m]^T, \qquad \mathbf{u} \in \mathbb{R}^m$$

$$\mathbf{y} = [y_1, y_2, \dots, y_m]^T, \qquad \mathbf{y} \in \mathbb{R}^m$$
(10)

$$\mathbf{u} = [u_1, u_2, \dots u_m]^T, \qquad \mathbf{u} \in \mathbb{R}^m \tag{10}$$

$$\mathbf{y} = [y_1, y_2, \dots, y_m]^T, \qquad \mathbf{y} \in \Re^m \tag{11}$$

 $f(\cdot)$ and $h(\cdot)$ are smooth nonlinear functions, and $(n,m) \in \mathbb{N}$. Moreover, it is assumed that $m \leq n$.

As depicted in Fig. 2, the nonlinear flat systems are equivalent to the linear controllable systems. A system is denoted flat if an output vector y exists, which fulfills the following

1) The output variables y_i can be stated as functions of the state variables x_i , the input variables u_i , and a finite number α of their time derivatives, i.e.

$$\mathbf{y} = \phi\left(\mathbf{x}, u, \dot{u}, \dots, u^{(\alpha)}\right). \tag{12}$$

2) All state variables x_i and all control inputs u_i can be stated as functions of the output variables y_i and a finite number β of their time derivatives, i.e.

$$\mathbf{x} = \varphi\left(y, \dot{y}, \dots, y^{(\beta)}\right) \tag{13}$$

$$\mathbf{u} = \psi\left(y, \dot{y}, \dots, y^{(\beta+1)}\right) \tag{14}$$

where $\phi(\cdot)$, $\varphi(\cdot)$, and $\psi(\cdot)$ are smooth mapping functions.

If the output variables of interest can be proven to be flat outputs y, the reference signal y_{REF} becomes straightforward.

IV. POWER CONTROL LOOP OF THE MULTIPHASE INTERLEAVED BOOST CONVERTER

A. Flatness of the Boost Converter

Controlling an interleaved multiphase converter is the same as controlling a single boost converter, but the uniqueness of the proposed method is the new control law. Based on the flatness principle introduced above, the input power of each converter cell p_L is assumed to be the flat output component. Thus, we define a flat output $y=p_L$, a control variable u=d, and a state variable $x=i_L$. From (3), the state variable x can be written as

$$x = \frac{p_L}{v_{\rm FC}} = \varphi(y). \tag{15}$$

From (1) and (7), the control variable u can be calculated from the flat output y and its time derivative \dot{y} , i.e.

$$u = 1 + \left(\dot{y} \cdot \frac{L}{v_{FC}} + R_L \cdot i_L - v_{FC}\right) \cdot \frac{1}{v_{Bus}} = d = \psi(\dot{y}). \tag{16}$$

It is apparent that $x = \varphi(y)$ and $u = \psi(\dot{y})$ correspond to (13) and (14), respectively. Consequently, the mathematical model of the converter can be considered as a flat system.

B. Control Law and Stability

The input-power reference of each module is represented by $y_{\rm REF}$ (= $p_{\rm LREF}$). A linearizing feedback control law achieving an exponential asymptotic tracking of the trajectory is given by the following expression [12], [16]:

$$(\dot{y} - \dot{y}_{REF}) + K_{11}(y - y_{REF}) + K_{12} \int_{0}^{t} (y - y_{REF}) d\tau = 0$$
(17)

where K_{11} and K_{12} are the controller parameters. One may set the following as a desired characteristic polynomial:

$$p(s)=s^2+2\zeta\omega_n s+\omega_n^2 \qquad K_{11}=2\zeta\omega_n \qquad K_{12}=\omega_n^2 \tag{18}$$

where ζ and ω_n are the desired dominant damping ratio and natural frequency, respectively.

Replacing the term for \dot{y} into (16) gives the equation for the closed-loop static-state feedback duty cycle d (called the *inverse dynamic equation*), where $e = y - y_{\rm REF}$, i.e.

$$u = 1 + \left(\left(\dot{y}_{REF} - K_{11}e - K_{12} \int_{0}^{t} e d\tau \right) \cdot \frac{L}{v_{FC}} + R_{L} \cdot i_{L} - v_{FC} \cdot \frac{1}{v_{Bus}} \right)$$

$$= \psi(\dot{y}) = d. \tag{19}$$

Clearly, the control system is stable for K_{11} , $K_{12} > 0$ $(\zeta, \omega_n > 0)$. Thus, the nonlinear-control law of the input power detailed above is portrayed in Fig. 3. The measured

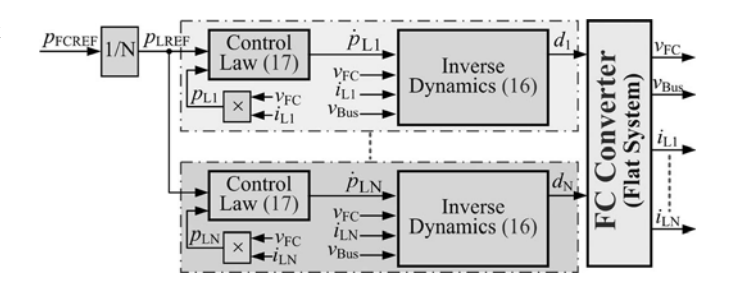


Fig. 3. Power-control loop based on the flatness principle of the multiphase boost converters

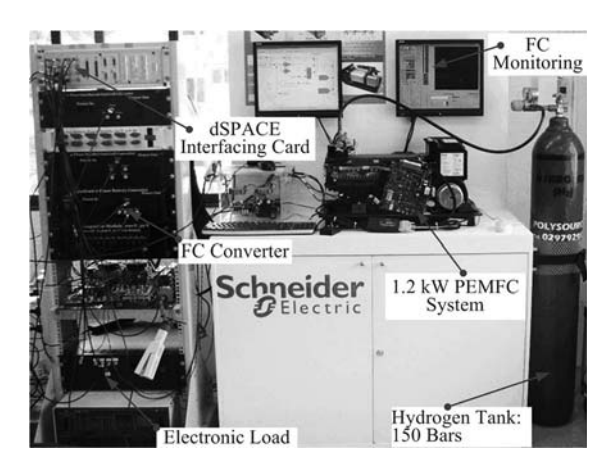


Fig. 4. Photograph of test-bench system.

TABLE I CONVERTER PARAMETERS AND SEMICONDUCTOR DEVICES

420 μH
$_{2,700}$ $_{\mu}$ F
IRFP264N: 250 V, 38 A
RURG3020: 200 V, 30 A

input powers of each module are carried out by means of (3) associated to a first-order filter used to reduce harmonics due to power-electronic switching. Based on the power-electronic constant switching frequency ω_S (PWM) and the cascade control structure, the outer control loop (here, the input-power control) must operate at a cutoff frequency $\omega_P \ll \omega_F$ (a cutoff frequency of the first-order filter) $\ll \omega_S$. Once the flat outputs are stabilized, the whole system is exponentially stable because all the variables of the system are expressed in terms of the flat outputs.

V. EXPERIMENTAL VALIDATION

A. Test-Bench Description

The small-scale test bench was implemented in the laboratory, as presented in Fig. 4. The four-phase boost converter parameters and semiconductor components are detailed in Table I. The FC system used in this effort was a PEMFC system (1.2 kW, 46 A, and based on Ballard Power Systems Inc.), as illustrated in Fig. 4. The power-control loops were implemented in the real-time card dSPACE DS1104 platform (see Fig. 4) using the fourth-order Runge-Kutta integration algorithm and a sampling time of $20~\mu s$, through the mathematical environment of MATLAB–Simulink.

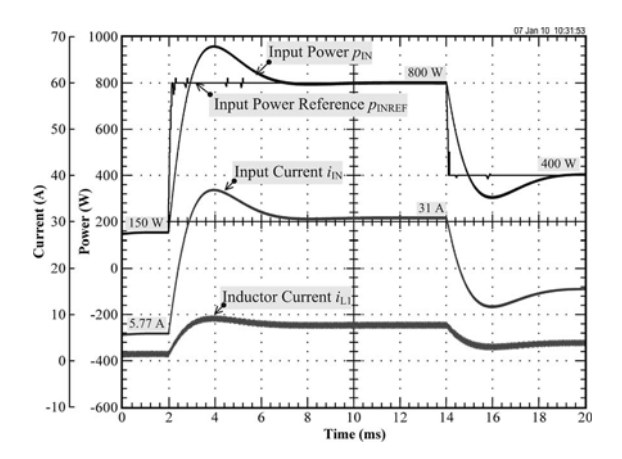


Fig. 5. Dynamic performance at an input-power reference $p_{\rm INREF}$ step from 150 to 800 W at t=2 ms and from 800 to 400 W at t=14 ms.

B. Experimental Results

1) FC Converter Testing With an Ideal Power Supply: Because the FC has slow dynamics by nature [17], an initial testing was performed using an ideal 26-V power supply (which has the same rated voltage as the FC) in place of the FC in order to confirm that the converter can operate correctly and to observe the dynamic performance of the proposed control law.

Fig. 5 presents waveforms that are obtained during the large step of the input-power setpoint. The nonlinear controller gains used were $K_{11}=1414~{\rm rd\cdot s^{-1}}$ and $K_{12}=1000\,000~{\rm rd^2\cdot s^{-2}}$ ($\zeta=0.707;~\omega_n=1000~{\rm rd\cdot s^{-1}}$). As a result, the cutoff frequency ω_P of the closed-loop input power was equal to $1000~{\rm rd\cdot s^{-1}}$, which is lower than the cutoff frequency ω_F of the measured power filter of $10\,000~{\rm rd\cdot s^{-1}}$ ($T_F=0.1~{\rm ms}$), so that the system was exponentially stable.

The data show the input-power reference p_{INREF} (instead of $p_{\rm FCREF}$), the input-power response $p_{\rm IN}$ (instead of $p_{\rm FC}$), the input current $i_{\rm IN}$ (instead of $i_{\rm FC}$) and the first inductor current i_{L1} . In the initial state, the input-power setpoint is equal to 150 W, the constant input voltage (instead of $v_{\rm FC}$) is equal to 26 V, and the dc bus voltage is equal to 60 V; as a result, the average input current is equal to around 5.77 A (150 W/26 V), and the first inductor current is equal around 1.44 A (150 W/4/26 V). At t = 2 ms, the input-power setpoint steps to the constant power of 800 W (positive transition), and at t = 14 ms, the input-power setpoint steps from 800 to 400 W (negative transition). The results reveal that, corresponding to the second-order dynamics [see (18)] of the observation error, the dynamic response is affected by this kind of large input command. The overshoot (no oscillations) in the inputpower response is due to a large proportional gain K_{11} of 1414 ${
m rd}\cdot {
m s}^{-1}$ and the vast setpoint step. The value of K_{11} can be reduced to attenuate the overshoot; however, this leads to a slower transition. Therefore, the present mathematical model of the power converter precisely predicts the dynamics of the control system.

2) FC Converter Testing With a PEMFC: Because the FC has slow dynamics by nature, only the constant input-power reference was performed. The oscilloscope waveforms in Fig. 6 portray the steady-state characteristics of the interleaved converters at the FC power reference of 500 W, the electronic load at the dc bus being adjusted in order to obtain a constant dc bus voltage of 60 V (here, the rated value). The data illustrate the

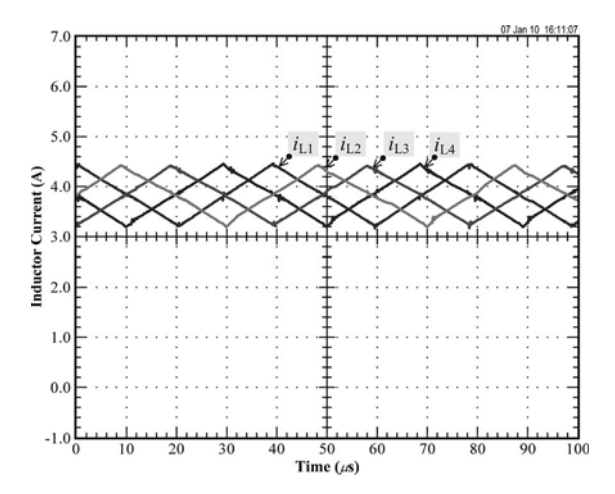


Fig. 6. Inductor-current waveforms of the converter at an FC power reference $p_{\rm FCREF}$ of 500 W $(v_{\rm Bus}=60~{\rm V},v_{\rm FC}=33.00~{\rm V},i_{\rm FC}=15.15~{\rm A},~{\rm and}~i_L=3.79~{\rm A}).$

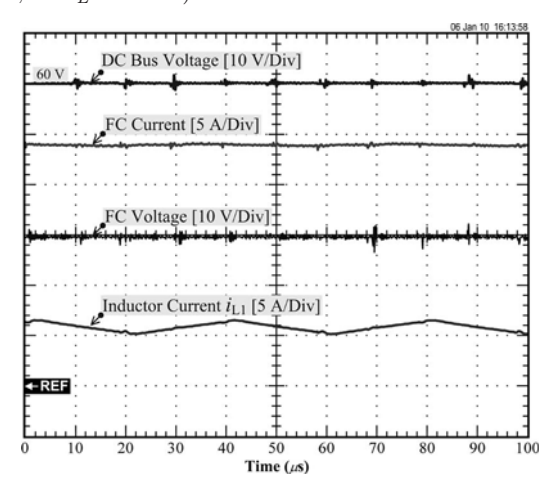


Fig. 7. Steady-state waveforms of the converter at an FC power reference $p_{\rm FCREF}$ of 700 W ($v_{\rm Bus}=60\,$ V, $v_{\rm FC}=30.00\,$ V, $i_{\rm FC}=23.80\,$ A, and $i_L=5.95\,$ A).

first, the second, the third, and the fourth inductor currents. One can observe that the paralleled interleaving-boost approach uses forced current sharing between the power stages to balance the power that the stages deliver.

As a final test, oscilloscope waveforms obtained during the FC power demand of 700 W are presented in Fig. 7. The data show the FC current, the dc bus voltage, the FC voltage, and the first inductor current i_{L1} . One can observe that the FC current is the sum of the inductor currents and that the FC ripple current is 1/N of the individual inductor ripple currents. It means that the FC mean current is close to the FC root-mean-square current.

VI. COMPARATIVE STUDY

To compare the performance of the flatness-based control, a traditional linear PI control method is also detailed. However, a current controller is classically implemented [3], [17] in place of the power controller. An inductor-current reference is represented by $i_{\rm LREF}$. A linear feedback PI control law is given by the following expression:

$$d = K_P(i_{\text{LREF}} - i_L) + K_I \int_0^t (i_{\text{LREF}} - i_L) d\tau$$
 (20)

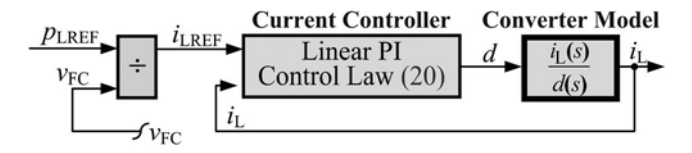


Fig. 8. Power-control loop based on a linear PI principle of the single-phase boost converters.

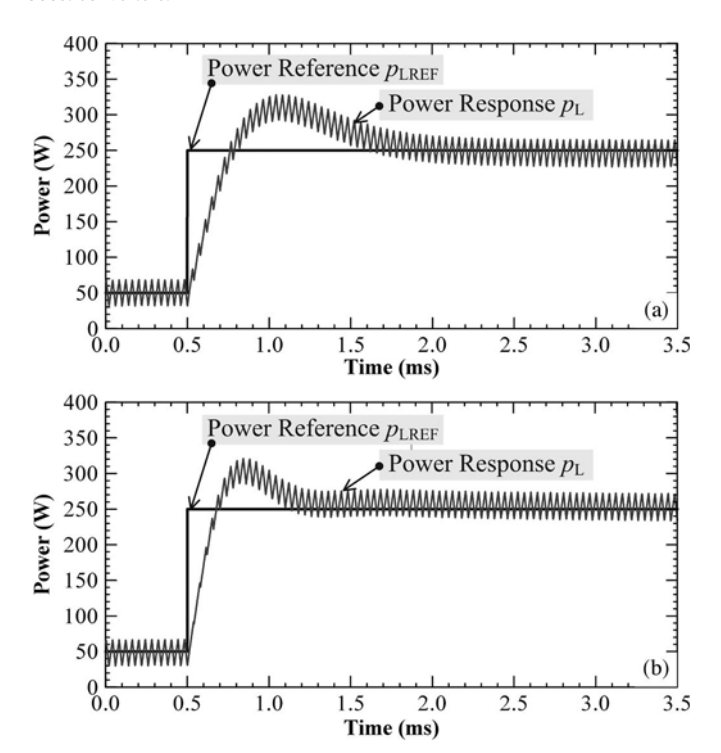


Fig. 9. Simulation results. Comparison of the flatness-based control law with a linear PI control law. (a) Linear PI and (b) flatness converter responses to a large step of the power reference from 50 to 250 W at $t=0.5\,\mathrm{ms}$.

where K_P and K_I are the set of controller parameters. Thus, the linear-control law of the power-control loop is portrayed in Fig. 8. It is similar to the nonlinear-control law (see Fig. 3), where the PI controller also generates a duty-cycle reference d. The main difference between the nonlinear control based on the flatness property and the classical linear control is that the inverse dynamic equation, known as the flatness property [see (16) and Fig. 3], appears in the nonlinear control.

To compare the performance of the flatness-based control and the linear PI control laws, the simulation was implemented. Simulations with MATLAB/Simulink were performed using a switching model of the boost converter. To give a reasonable comparison between the methods, the parameters of the linear PI controller K_P and K_I were tuned to obtain the best possible performance, and this result is compared with the flatness-based control. Then, $K_P=0.15~\mathrm{A}^{-1}$, and $K_I=200~\mathrm{(A\cdot s)}^{-1}$.

Fig. 9 shows the simulation results obtained for both controllers during the large step of the power reference. It is similar to the test-bench results illustrated in Fig. 5. The flatness-based control shows a better dynamic response. Although the dynamic response of the linear-control law could be improved relative to that shown in Fig. 9, this enhancement came at the expense of a reduced stability margin. From these results, we conclude that the flatness-based control provides a better performance than the classical PI controller.

VII. CONCLUSION

The main contribution of this brief is to model and control a nonlinear switching-power converter. Distributed power systems often invoke the need to parallel power converters for a variety of reasons, i.e., enhanced reliability, enabling the use of standardized designs with varying loads, distributing heat sources, and improved maintainability. The proposed converter is four-phase parallel step-up converters with the interleaved switching technique. Controlling an interleaved multiphase converter is the same as controlling a single boost converter, but the uniqueness of the proposed method is the new control law. Using the nonlinear-control approach based on the flatness property, we have proposed a simple solution to the optimization and stabilization problems in the nonlinear power-electronic system. This is the novel concept for this kind of application.

REFERENCES

- J. Bernard, S. Delprat, F.-N. Büchi, and T.-M. Guerra, "Fuel-cell hybrid powertrain: Toward minimization of hydrogen consumption," *IEEE Trans. Veh. Technol.*, vol. 58, no. 7, pp. 3168–3176, Sep. 2009.
- [2] P. Thounthong, B. Davat, S. Raël, and P. Sethakul, "Fuel cell high-power applications," *IEEE Ind. Electron. Mag.*, vol. 3, no. 1, pp. 32–46, Mar. 2009.
- [3] J. Zou, X. Ma, and C. Du, "Asymmetrical oscillations in digitally controlled power-factor-correction boost converters," *IEEE Trans. Circuits Syst. II, Exp. Brief*, vol. 56, no. 3, pp. 230–234, Mar. 2009.
- [4] P. Thounthong, S. Raël, and B. Davat, "Analysis of supercapacitor as second source based on fuel cell power generation," *IEEE Trans. Energy Convers.*, vol. 24, no. 1, pp. 247–255, Mar. 2009.
 [5] S. Ozeri, D. Shmilovitz, S. Singer, and L. M. Salamero, "The mathemat-
- [5] S. Ozeri, D. Shmilovitz, S. Singer, and L. M. Salamero, "The mathematical foundation of distributed interleaved multiple systems," *IEEE Trans. Circuits Syst. I, Reg. Papers*, vol. 54, no. 3, pp. 610–619, Mar. 2007.
- [6] F. Amato, C. Cosentino, A. S. Fiorillo, and A. Merola, "Stabilization of bilinear systems via linear state-feedback control," *IEEE Trans. Circuits Syst. II, Exp. Brief*, vol. 56, no. 1, pp. 76–80, Jan. 2009.
- [7] M. Hajian, G. R. Arab Markadeh, J. Soltani, and S. Hoseinnia, "Energy optimized sliding-mode control of sensorless induction motor drives," *Energy Convers. Manage.*, vol. 50, no. 9, pp. 2296–2306, Sep. 2009.
- [8] V. Kumar, R. R. Joshi, and R. C. Bansal, "Optimal control of matrix-converter-based WECS for performance enhancement and efficiency optimization," *IEEE Trans. Energy Convers.*, vol. 24, no. 1, pp. 264–273, Mar. 2009.
- [9] F. U. Syed, M. L. Kuang, M. Smith, S. Okubo, and H. Ying, "Fuzzy gain-scheduling proportional-integral control for improving engine power and speed behavior in a hybrid electric vehicle," *IEEE Trans. Veh. Technol.*, vol. 58, no. 1, pp. 69–84, Jan. 2009.
- [10] M. Fliess, J. Lévine, Ph. Martin, and P. Rouchon, "A Lie–Bäcklund approach to equivalence and flatness of nonlinear systems," *IEEE Trans. Autom. Control*, vol. 44, no. 5, pp. 922–937, May 1999.
- [11] M. A. Danzer, J. Wilhelm, H. Aschemann, and E. P. Hofer, "Model-based control of cathode pressure and oxygen excess ratio of a PEM fuel cell system," *J. Power Sources*, vol. 176, no. 2, pp. 515–522, Feb. 2008.
- [12] E. Song, A. F. Lynch, and V. Dinavahi, "Experimental validation of non-linear control for a voltage source converter," *IEEE Trans. Control Syst. Technol.*, vol. 17, no. 5, pp. 1135–1144, Sep. 2009.
- [13] A. Gensior, H. Sira-Ramirez, J. Rudolph, and H. Guldner, "On some nonlinear current controllers for three-phase boost rectifiers," *IEEE Trans. Ind. Electron.*, vol. 56, no. 2, pp. 360–370, Feb. 2009.
- [14] T. Rabbani, S. Munier, D. Dorchies, P. Malaterre, A. Bayen, and X. Litrico, "Flatness-based control of open-channel flow in an irrigation canal using SCADA," *IEEE Control Syst. Mag.*, vol. 29, no. 5, pp. 22–30, Oct. 2009.
- [15] S. K. Agrawal, K. Pathak, J. Franch, R. Lampariello, and G. Hirzinger, "A differentially flat open-chain space robot with arbitrarily oriented joint axes and two momentum wheels at the base," *IEEE Trans. Autom. Con*trol, vol. 54, no. 9, pp. 2185–2191, Sep. 2009.
- [16] A. Payman, S. Pierfederici, and F. Meibody-Tabar, "Energy control of supercapacitor/fuel cell hybrid power source," *Energy Convers. Manage.*, vol. 49, no. 6, pp. 1637–1644, Jun. 2008.
- [17] P. Thounthong, B. Davat, S. Raël, and P. Sethakul, "Fuel starvation: Analysis of a PEM fuel cell system," *IEEE Ind. Appl. Mag.*, vol. 15, no. 4, pp. 52–59, Jul./Aug. 2009.